

1 **Spatial-temporal changes in flow hydraulic characteristics and soil loss**
2 **during gully headcut erosion under controlled conditions**
3

4 Mingming Guo^a, Zhuoxin Chen^b, Wenlong Wang^{b,c,*}, Tianchao Wang^d, Qianhua Shi^b, Hongliang
5 Kang^b, Man Zhao^b, Lanqian Feng^c
6

7 a Key laboratory of Mollisols Agroecology, Northeast Institute of Geography and Agroecology,
8 Chinese Academy of Sciences, Harbin 150081, Heilongjiang, China

9 b State Key Laboratory of Soil Erosion and Dryland Farming on the Loess Plateau, Institute of Water
10 and Soil Conservation, Northwest A&F University, Yangling, Shaanxi 712100, China

11 c Institute of Soil and Water Conservation, Chinese Academy of Sciences and Ministry of Water
12 Resources, Yangling, Shaanxi 712100, China

13 d Ulanyab Grassland Station, Jining, Inner Mongolia 012000, China

14 ***Corresponding author:** Wenlong Wang

15 E-mail addresses: nwafu_wwl@163.com; wllwang@nwsuaf.edu.cn
16

17 **Abstract**

18 The temporal-spatial changes in flow hydraulics and energy consumption and their associated soil
19 erosion remain unclear during gully headcut retreat. A simulated scouring experiment was conducted
20 on five headcut plots consisting of upstream area (UA), gully headwall (GH) and gully bed (GB) to
21 elucidate the temporal-spatial changes in flow hydraulic, energy consumption, and soil loss during
22 headcut erosion. The flow velocity at the brink of headcut increased as a power function of time,
23 whereas the jet velocity entry to plunge pool and jet shear stress logarithmically or linearly decreased
24 over time. The jet properties were significantly affected by upstream flow discharge. The Reynold
25 number, runoff shear stress, and stream power of UA and GB increased as logarithmic or power
26 functions of time, but the Froude number decreased logarithmically over time. The Reynold number,
27 shear stress and stream power decreased by 56.0%, 63.8% and 55.9%, respectively, but the Froude
28 number increased by 7.9% when flow dropped from UA to GB. The accumulated energy
29 consumption of UA, GH and GB positions linearly increased with time. 91.12% - 99.90% of total
30 flow energy was consumed during headcut erosion, of which the gully head accounted for 77.7% of
31 total energy dissipation followed by UA (18.3%) and GB (4.0%). The soil loss rate of the
32 “UA-GH-GB” system initially rose and then gradually declined and levelled off. The soil loss of UA
33 and GH decreased logarithmically over time, whereas the GB was mainly characterized by sediment
34 deposition. The proportion of soil loss at UA and GH are 11.5% and 88.5%, respectively, of which
35 the proportion of deposited sediment on GB reached 3.8%. The change in soil loss of UA, GH and
36 GB was significantly affected by flow hydraulic and jet properties. The critical energy consumption
37 initiating soil erosion of UA, GH, and GB are 1.62 J s^{-1} , 5.79 J s^{-1} and 1.64 J s^{-1} , respectively. These
38 results are helpful to deepen the understanding of gully erosion process and hydrodynamic
39 mechanism and also can provide scientific basis for the construction of gully erosion model and the
40 design of gully erosion prevention measures.

41
42 **Keywords:** Gully erosion; Hydraulic property; Headcut retreat; Mass failure; Energy dissipation

43

44 **1 Introduction**

45 Gully erosion is a typical soil erosion process whereby concentrated runoff from an upstream
46 drainage area recurs in a channel and erodes soil from the area through which runoff passed to
47 considerable depth (Poesen et al., 2003; Zhu, 2012). Gully erosion is recognized as the main
48 sediment source in some hilly and gully-dominated watersheds (Poesen et al., 2003; Valentin et al.,
49 2005; Dotterweich et al., 2012). Poesen et al. (2003) reported that soil loss amount caused by gully
50 erosion accounts for 10% - 94% of total soil loss amount based on the collected data from published
51 articles. Moreover, gully erosion can severely damage to infrastructure, enhance the terrain
52 fragmentation, and cause ecosystem instability, land degradation and food safety (Vanmaercke et al,
53 2016; Zhang et al., 2018; Hosseinalizadeh et al., 2019; Arabameri et al., 2020; Bogale et al., 2020;
54 Belayneh et al., 2020; Wen et al., 2020).

55 As the primary process of the gully erosion, the gully headcut retreat often significantly
56 influences and determines gully erosion (Oostwoud-Wijdenes et al., 2000; Vandekerckhove et al.,
57 2003; Guo et al., 2019). A headcut is defined as a vertical or near-vertical drop or discontinuity on
58 the bed of a gully occurring where flow is concentrated at a knickpoint (Hanson et al., 2001; Bennett
59 et al., 2000). Many studies have demonstrated that the gully erosion is the result of the combined
60 actions of plunge pool erosion by jet flow, upstream runoff incision, headwall erosion by on-wall
61 flow, mass failure (of gully head and wall collapse), (Vanmaercke et al., 2016; Addisie et al., 2017;
62 Guo et al., 2019). Once a headcut is formed in upstream area, the gully will develop rapidly and not
63 stop forward until a critical topographic condition is formed ($S \leq a \cdot A^b$, where S and A is the slope
64 gradient and drainage area upstream gully headcut, respectively) (Kirkby et al., 2003). Moreover, the
65 different landform units (upstream area, UA; gully head, GH; gully bed, GB) of gully system
66 exhibited— completely different erosion processes and hydrodynamic mechanisms during gully
67 headcut erosion (Zhang et al., 2018; Guo et al., 2019; Shi et al., 2020a). The combination and
68 interaction of erosion processes of the three landform units determined gully headcut erosion process
69 (Vanmaercke et al., 2016). Therefore, clarifying the soil erosion process and characteristics of the
70 three landform units is critical to systematically and clearly reveal the mechanism of gully headcut
71 erosion.

72 Previous studies suggested that gully headcut erosion is affected by various factors including
73 topography, land use change, vegetation, soil properties, and climate (Vanwalleggem et al., 2003;
74 Ionita, 2006; Rodzik et al., 2009; Rieke-Zapp and Nichols, 2011; Torri and Poesen, 2014; Ionita et al.,
75 2015; Vannoppen et al., 2015; Guo et al., 2019, 2020a). In terms of topography, most of studies
76 focused on the threshold relationship ($S \leq a \cdot A^b$) to initiate gully erosion (e.g., Torri and Poesen, 2014).
77 Several experimental studies demonstrated that the upstream slope gradient and headcut height have
78 significant effects on headcut erosion (e.g., Bennett, 1999; Zhang et al., 2018). Land use change is
79 recognized as having the strongest effect on processes related to gully erosion (Poesen et al., 2003;
80 Chaplot et al., 2005; Descroix et al., 2008), and also significantly affects the activation of gully
81 headcut erosion (e.g., Torri and Poesen, 2014). In this aspect, the vegetation coverage is a parameter
82 that is often used to clarify its effect on gully erosion (e.g., De Baets et al., 2007;
83 Martínez-Casasnovas et al., 2009), however, in fact, the vegetation effect mainly depends on the root
84 characteristics and its distribution at gully head (e.g., Vannoppen et al., 2015; Guo et al., 2019).
85 Nevertheless, at present, the most of studies on gully erosion focus on the changes in gully
86 morphology between different periods at a watershed or regional scale (Vanmaercke et al., 2016),
87 which is why the previous studies fail to address the effects of root systems on gully headcut retreat.
88 Guo et al. (2019) concluded that the grass (*Agropyron cristatum*) could reduce soil loss and headcut
89 retreat distance by 45.6–68.5%, 66.9–85.4%, respectively, compared with bare land, and the roots of
90 0–0.5 mm in diameter showed the greatest controlling influence on headcut erosion. In terms of soil
91 properties, lots of studies have proved the significant effect of soil properties on gully headcut
92 erosion (e.g., Nazari Samani et al., 2010), which is mainly related to the change in soil erodibility
93 induced by soil properties including soil texture, soil vertical joints, soluble mineral content, soil
94 lithology, and physicochemical properties (Sanchis et al., 2008; Vanmaercke et al., 2016; Guo et al.,
95 2020a). Rainfall, the main climate factor, is closely related to runoff generation and thus be expected
96 to affect headcut erosion. Many studies have reported that the initiation of gully headcut is correlated
97 with rainfall characteristics (e.g., summation of rainfall from 24-hour rains equal to or greater than
98 0.5 inches) (Beer and Johnson, 1963; Vandekerckhove et al., 2003; Rieke-Zapp and Nichols, 2011).
99 However, the great difference in the threshold value relating to rainfall factors was found among

100 different areas of the world due to fully different erosion environments. For example, in the northeast
101 of China, the gully erosion is the result of soil thawing, rainfall runoff and snowmelt runoff (Li et al.,
102 2016b; Xu et al., 2019). Furthermore, at present, the most of studies on gully erosion were conducted
103 to quantify the change in gully erosion (retreat rate, area and volume) at different spatial and
104 temporal scales by using remote sensing interpretation, real-time monitoring and meta-analysis based
105 on literature data (e.g., Vanmaercke et al., 2016). However, the influencing mechanism of these
106 factors on gully headcut erosion is still unclear and need to be revealed in future studies.

107 Evidently, the concentrated flow upstream gully head, mainly depended on the drainage area
108 upstream gully heads and rainfall characteristics, is the main and original drive force triggering
109 headcut erosion. The runoff firstly eroded the upstream area and then was parted into two types of
110 flow (on-wall flow and jet flow) at the brinkpoint of gully headcut (Guo et al., 2021a). Consequently,
111 the on-wall flow persistently eroded ~~the~~ headwall soil, and the jet flow violently impacted gully bed
112 soil and formed a plunge pool (Su et al., 2015; Guo et al., 2019). Subsequently, the two types of flow
113 merged again and eroded gully bed together (Zhang et al., 2018; Shi et al., 2020a). The runoff
114 hydraulic or jet flow properties at different landform units (~~upstream area~~UA, ~~gully head~~GH and
115 ~~gully bed~~GB) are significantly different, which is an important reason for the difference in erosion
116 process among different landform units. However, the temporal-spatial change in runoff and jet
117 properties during headcut erosion is still unclear and thus needs to be clarified. Furthermore, at
118 present, some experimental studies on headcut erosion of rill, ephemeral gully, gully and bank gully
119 were conducted to investigate the runoff properties, energy consumption, sediment transport process,
120 morphology evolution and empirical model (Bennett and Casali, 2001; Wells et al., 2009a, 2009b; Su
121 et al., 2014; Xu et al., 2017a; Guo et al., 2019; Shi et al., 2020a). However, relatively few
122 knowledges were obtained to systemically reveal the hydrodynamic mechanism of gully headcut
123 erosion. Therefore, elucidating the temporal-spatial changes in runoff hydraulic and soil loss and
124 hydrodynamic mechanism of UA, GH and GB is of great importance to systematically reveal the
125 hydrodynamics mechanism of gully headcut erosion.

126 Given the above-mentioned issues, a series of simulated gully headcut erosion experiments
127 subjected to inflow scouring are conducted to (1) investigate the temporal-spatial change in runoff

128 hydraulic and jet flow properties during headcut erosion, (2) quantify the dynamic change of energy
129 consumption and soil loss and their spatial distribution, and (3) reveal the erosion hydrodynamic
130 mechanism of UA, GH and GB.

131 **2 Materials and Methods**

132 **2.1 Study area**

133 This experiment was carried out at the Xifeng Soil and Water Conservation Experimental
134 Station that is located in the Nanxiaohegou watershed, Qingyang City, Gansu Province, China. The
135 study area belongs to a semi-arid continental climate with a mean annual temperature of 9.3 °C. The
136 mean annual precipitation is 546.8 mm (1954 - 2014), of which precipitation from May to September
137 accounts for 76.9% of the total precipitation (Xia et al., 2017; Guo et al., 2019). The elevation ranges
138 from 1050 to 1423 m. The main landforms include gentle loess-tableland, steep hillslope and gully
139 channel, and their areas account for 57.0%, 15.7% and 27.3%, respectively. The loess-tableland is
140 characterized by low slope (1--5°), gentle and flat terrain and fertile soil. The main soil type is
141 loessial soil with silt loam texture. Most of hillslopes have been constructed as slope-terraces. The
142 main gully channel is usually U-shaped and the branch-gully is more actively developed and easily
143 eroded as a V-shaped by runoff from loess-tableland (Xu et al., 2019). The flat loess-tableland can
144 accumulate the 67.4% of total runoff and cause serious gully erosion that can contribute 86.3% of the
145 total soil erosion (Guo et al., 2019). The original plant species have been seriously destroyed. Since
146 the 1970s, the “Three Protection Belts” system, the “Four Eco-Economical Belts” system and the
147 “Grain for Green” project (Zhao, 1994; Fu et al., 2011) were implemented to control soil erosion.
148 The main land use on loess-tableland position has always been farmland and orchards, while the land
149 use on hillslope is sloping farmland and orchards before 1999, which have been changed into
150 forested and grassy land due to the “Grain for Green” project. The current mean annual soil erosion
151 rate has been reduced to 4350 Mg km⁻² y⁻¹ in the study watershed (Guo et al., 2019). The plants are
152 primarily artificially planted arbors and herbaceous vegetation and shrubs (Guo et al., 2021b).

153

154 2.2 Experimental design

155 2.2.1 Gully head experimental plot construction

156 Five gully head plots for headcut erosion experiments were constructed at the experimental
157 station in April 2018. Fig. 1 shows the basic information of the gully head plot consisting of three
158 landform units (upstream area, headwall and gully bed). The plot width and slope gradient of
159 upstream area and gully bed are uniformly designed as 1.5 m and 3°, respectively. The upstream area
160 length, the height of the vertical headwall and the length of the gully bed are 5.0 m long, 0.9 m, and
161 1.0 m, respectively (Fig. 1a). The plot boundary was constructed in strict accordance with designed
162 plot dimension using cement and bricks (Fig. 1b). After the construction of plot boundary, the soil
163 was sieved through a 2 cm sieve ~~with~~ to remove roots and debris and ensure uniform soil underlying
164 condition. The sieved soil was filled into the plot every 10-cm thick layer according to the
165 investigated soil bulk density of gully heads. The soil surface of each layer was harrowed to increase
166 the cohesion between two soil layers (Guo et al., 2019). In general, the filling upstream area length
167 was 5.5 m that was larger than the precise upstream area length (5.0 m). After establishment of gully
168 head plots, the five plots were carefully managed about four months (August 2018) to allow the soil
169 to return to its nearly natural state. During the four-month conservation process, the naturally
170 growing weeds were weeded out in time. Moreover, a flow-steady tank of 0.6 m, 1.5 m and 0.5 m in
171 length, width and height was installed at the top of upstream area, and a circular sampling pool of 0.6
172 m in diameter was set at the bottom of the gully bed to collect runoff and sediment (Fig. 1a).
173 According to the pre-experimental results, the length of upstream area can meet the needs of headcut
174 migration under designed flow discharge ($3.0 \text{ --- } 7.2 \text{ m}^3 \text{ h}^{-1}$) and gully head height (0.9 m), and the
175 length of gully bed also can satisfy the development of plunge pool by jet flow and stabilize the flow
176 of gully bed.

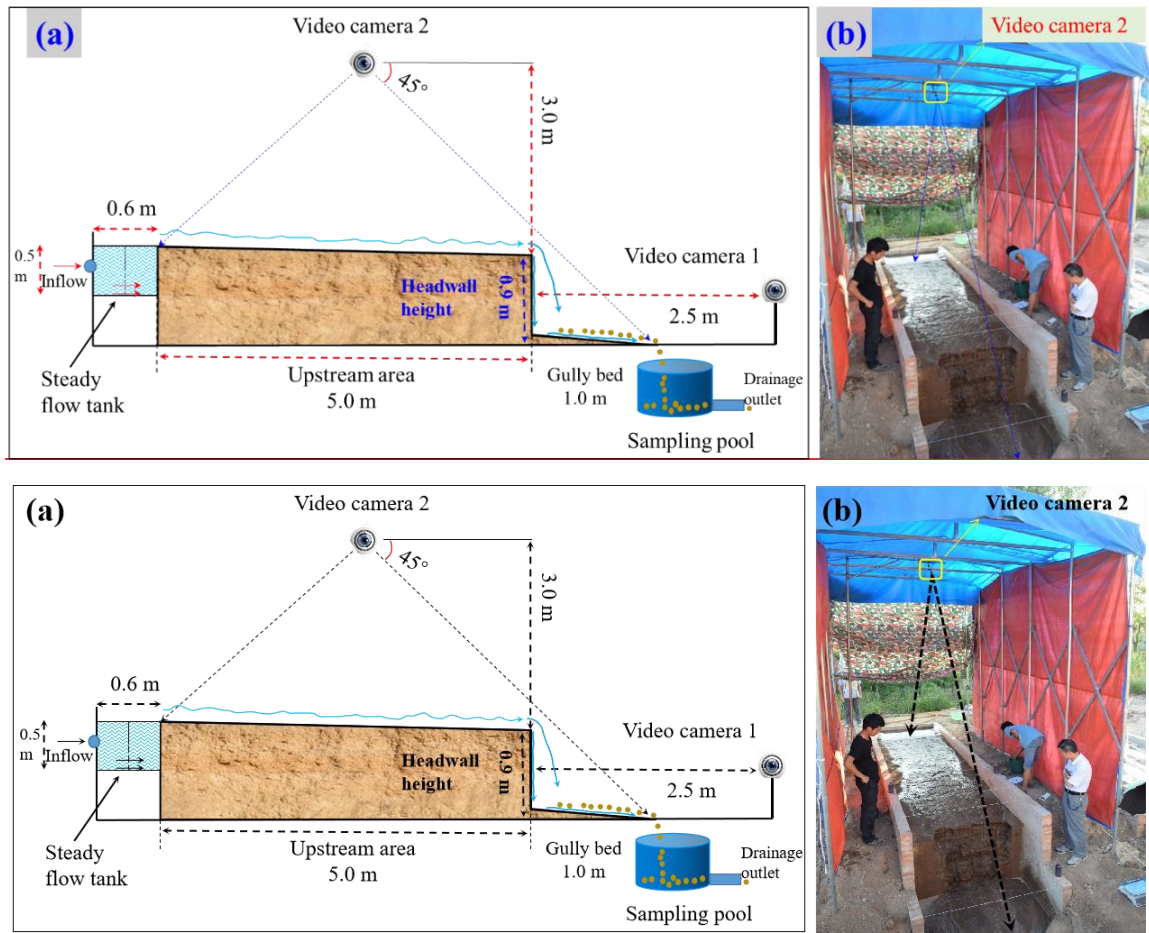


Figure 1. Sketch (a) and photo (b) of experimental plot.

2.2.2 Inflow discharge design

The concentrated runoff generated from upstream area is the main force driving gully headcut erosion. Jiao et al (1999) concluded that the more serious soil erosion is generally caused by “A” type rainstorm with the rainfall duration of 25 to 178 mins than other types of rainstorms in the Loess Plateau. Thus, an extreme case of rainfall duration (180 min) was considered in this study, and the recurrence period of “A” type rainstorm was designed as 30 years. Previous studies indicated that the rainstorm distribution on the Loess Plateau showed a non-significant change in past decades (Li et al., 2010; Sun et al., 2016; Wen et al., 2017). Zhang et al. (1983) proposed a statistical equation (Eq. (1)) for calculating the average rainfall intensity by analyzing 1710 typical rainstorm events in the Loess Plateau. Then, the inflow discharge was calculated by Eq. (2) that involves the runoff coefficient, storm intensity and drainage area upstream gully head and ranged from 3.12 to 9.68 m³ h⁻¹. Before the study, we first conducted some preliminary experiments under some flow discharges, and

193 meanwhile considering the pre-experiment effect, finally, we selected the five inflow discharge levels
194 (3.0, 3.6, 4.8, 6.0, and 7.2 m³ h⁻¹).

$$195 \quad RI = \frac{5.09N^{0.379}}{(t+1.4)^{0.74}} \quad (1)$$

196 where RI is the average rainfall intensity during t minutes, mm min⁻¹; N is the recurrence period
197 of rainstorm, yr; and t is the rainfall duration, min.

$$198 \quad q = \frac{60\alpha \cdot A \cdot RI \cdot w}{W} \quad (2)$$

199 where A is the upstream area (km²) and has a wide range of 0.15 - 8.7 km² according to an early
200 investigation of research team (Che, 2012); W is the width of the upstream area, km; w is the plot
201 width, m; and α is the runoff coefficient of bare land and is identified as 0.167 by analyzing the
202 runoff and rainfall data of standard runoff plots (Li et al., 2006).

203 **2.3 Experimental procedure**

204 The scouring experiment was conducted in August 2018. Before formal experiment, the
205 upstream area length was firstly adjusted to designed length of 5.0 m (Fig. 2a). Then, a self-made
206 tent (length × width × height: 6.0 m × 3.0 m × 3.5 m) with waterproof canvas enclosed the plot to
207 resist the effects of natural rainfall and sunshine on experimental progress and photo shooting for 3D
208 reconstruction (Fig. 1b). In addition, the experimental process was recorded by two Logitech 930e
209 video cameras with a resolution of 2.0 megapixels. The camera 1 was installed 2.5 m in front of plot
210 headwall (Fig. 1a), and the camera 2 was installed 3.0 m above the plot center (Fig. 1a).

211 Before the experiment, watering can be used to spray each experimental plot until surface runoff
212 was generated, and then the plot was placed for 24 hours to ensure adequate water infiltration, which
213 can assure that the soil moisture of the five plots was approximately the same. The inlet pipeline was
214 placed in steady flow tank when the inflow discharge was adjusted to designed value. A water
215 thermometer was placed into the steady flow tank to monitor the change in water temperature during
216 experiments. The runoff and sediment samples at the plot outlet were collected at 2-min intervals to
217 represent the temporal change in runoff and sediment of “UA—GH—GB” system, and the
218 sampling time was recorded using a stopwatch (Fig. 2b). The runoff and sediment samples were
219 oven-dried at 105 °C for 24 h and weighed to calculate the soil loss rate of “UA—GH—GB”
220 system. Besides, the timing of the collapse event was recorded during headcut erosion. The upstream

221 area was divided into 4 runoff observation sections, and the runoff width (w), depth (d) and velocity
 222 (V) of each section were measured by a calibrated scale of 1 mm accuracy and color tracer method
 223 (Fig. 2b, 2c). The runoff velocity (V_j) before runoff arrived at the brink of headcut was measured 5 –
 224 8 times by the flow velocity measuring instrument (LS300-A). The instrument was firstly placed
 225 perpendicular to the flow section but does not touch the underlying surface. When the flow passes
 226 through the turbine, the flow velocity can be measured by the rotating velocity of the turbine with the
 227 accuracy of 0.01 m s^{-1} and measuring error of $< 1.5\%$, and the runoff width at the headcut brinkpoint
 228 was measured (Fig. 2d). The runoff width and velocity of gully bed were also measured using the
 229 same method with upstream area (Fig. 2e). Above mentioned measurements of runoff characteristics
 230 and sediment samples were finished in 2-min intervals. The whole experimental process was
 231 recorded by two video cameras and imported into computers (Fig. 2f). In addition to above runoff
 232 parameters, the runoff depth (d_b) at the brink of headcut, the plunge pool depth (D_H) and the vertical
 233 distance (h) from brink-point of headcut to water surface of plunge pool were also measured 3 - 5
 234 times by a steel ruler with 1 mm accuracy within each 2-min intervals (Fig. 3).





236

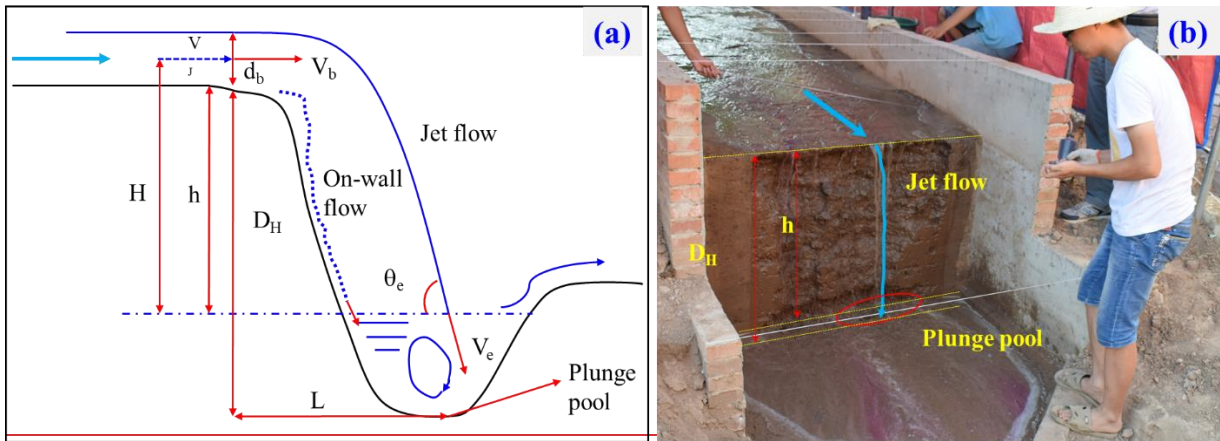
237

238

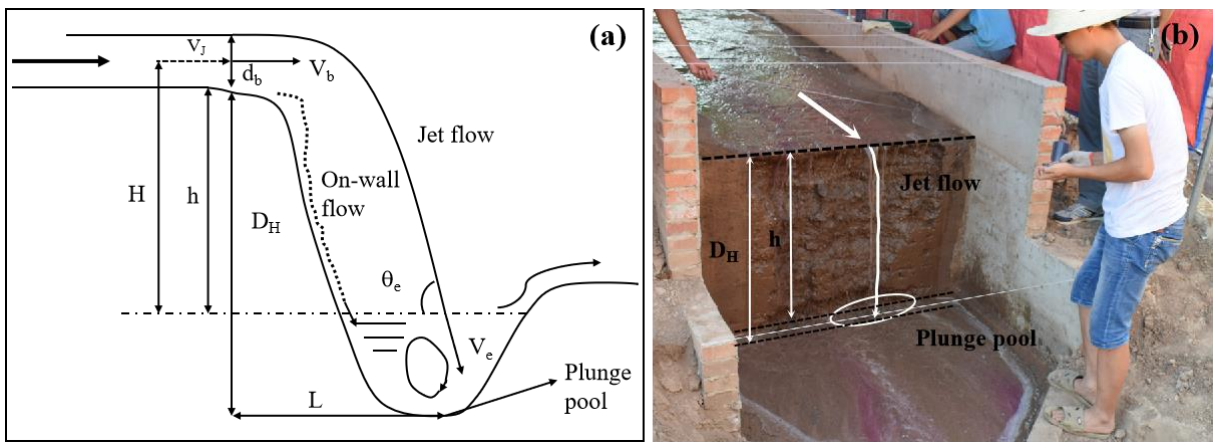
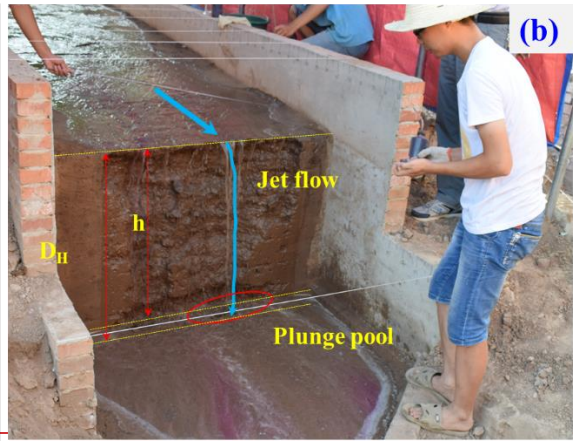
239

240

Figure 2. Plot construction (a), Runoff runoff width measurement of loess-tableland and runoff and sediment sampling of outlet (b) observation, runoff velocity measurement of loess-tableland (c), jet velocity measurement of gully head (d), runoff velocity and width measurement of gully bed (e), and experimental process recoding (f) at upstream area, gully head and gully bed.



241



242

243

244

Figure 3. Sketch of jet flow at gully headcut (a) and plunge pool at gully bed (b).

To obtain the dynamic change in morphology of erosional landform during gully headcut

245 erosion, the experimental duration (180 min) was divided into six stage (30 — 60 — 90 — 120 —
 246 150 — 180 min). Photo-based three-dimensional (3D) reconstruction method was employed to
 247 obtain the digital elevation model (DEM) data of each plot prior to experiment and after each 30-min
 248 test. A total of 14 target points were placed around the plot for identifying the 3D coordinate before
 249 the photos were taken. The eroded photographic was recorded by a Nikon D5300 camera with the
 250 focal length of 50 mm. The following aspects were required during photos shooting: (1) obvious
 251 water on soil surface and direct sunshine should be avoided, (2) a minimum overlap of 60% between
 252 subsequent photographs was required, and (3) some complex eroded photographic should be taken in
 253 detail. In this study, the upper left corner of the plot was set as the original coordinates (0, 0, 0), and
 254 the direction of three-dimensional coordinate was determined as shown in Fig. 3d. These collected
 255 photos were imported in Agisoft PhotoScan software (Agisoft LLC, Russia, professional version
 256 1.1.6), and then these control points and their coordinates would be identified and entered into the
 257 software. The root mean square errors for the altitudes (Z axis) of the target points are 0.0037, 0.0045,
 258 0.0024, 0.0052 and 0.0030 m on average, respectively, for the experiments of five inflow discharges,
 259 which can satisfy the study requirement (millimeter level). The DEM could be exported and was
 260 used to extract the morphological parameters and soil loss volume of three landform units at six
 261 stages (Frankl et al., 2015).

262 **2.4 Parameter calculation, data analysis and figure plotting**

263 **2.4.1 Hydraulic parameters of upstream area and gully bed**

264 Five parameters including runoff velocity (V , m s^{-1}), Reynold number (Re), Froude number (Fr),
 265 shear stress (τ , Pa) and stream power (ω , W m^{-2}) were used to characterize the changes in hydraulic
 266 properties at upstream area and gully bed positions. The several parameters except for V are
 267 calculated as follows.

$$268 \quad Re = \frac{V \cdot R}{\nu} \quad (1)$$

$$269 \quad Fr = \frac{V}{\sqrt{g \cdot R}} \quad (2)$$

$$270 \quad R = \frac{w \cdot d}{w + 2d}, \nu = \frac{1.775 \times 10^{-6}}{1 + 0.0337T + 0.000221T^2} \quad (3)$$

$$271 \quad \tau = \rho_w \cdot g \cdot R \cdot J \quad (4)$$

$$272 \quad \omega = \tau \cdot V \quad (5)$$

273 where R (m) and ν ($\text{m}^2 \text{s}^{-1}$) are the hydraulic radius and the water kinematic viscosity coefficient,
 274 respectively; w (m), d (m) and T ($^{\circ}\text{C}$) are the runoff width, depth and water temperature, respectively;
 275 ρ_w (kg m^{-3}) is the water density and J (m m^{-1}) is the hydraulic gradient.

276 2.4.2 Jet properties of gully head

277 Based on the measured runoff velocity (V_J , m s^{-1}) before runoff arrived at the headcut brinkpoint,
 278 the runoff depth (d_b , m) at the headcut brinkpoint, the plunge pool depth (D_H , m) and the vertical
 279 distance (h , m) (Fig. 3a), the three parameters including the runoff velocity at the headcut brinkpoint
 280 (V_b), jet-flow velocity entry to plunge pool (V_e) and jet-flow shear stress (τ_j) were calculated to
 281 clarify the change of jet properties (Rouse, 1950; Hager, 1983; Stein et al., 1993; Flores-Cervantes et
 282 al., 2006; Zhang et al., 2016). The three parameters were calculated as follows.

$$283 V_b = \begin{cases} \frac{\sqrt[3]{q \cdot g}}{0.715}, Fr < 1 \\ V_J \cdot \frac{Fr^2 + 0.4}{Fr^2}, Fr > 1 \end{cases} \quad (5)$$

$$284 Fr = \frac{V_J}{\sqrt{g \cdot d_b}} \quad (6)$$

$$285 V_e = \frac{V_b}{\cos \theta_e}, \theta_e = \arctan \left(\frac{\sqrt{2g \cdot D_H}}{V_b} \right) \quad (7)$$

$$286 \tau_j = 0.025 \left(\frac{v}{q} \right)^{0.2} \cdot \rho_w \cdot [2g \cdot (h + d_b/2) + V_b^2] \quad (8)$$

287 2.4.3 Energy consumption of upstream area, gully head and gully bed

288 In this study, energy consumption of three landform units (~~upstream area, UA;~~, ~~gully head,~~
 289 ~~GH;~~, ~~gully bed, GB~~) were calculated according to the measured runoff characteristic parameters.
 290 The bottom of GB was treated as the zero potential surface to quantify the energy consumption.
 291 Therefore, the total runoff energy (E_T , J s^{-1}), the runoff energy at the brink of headcut (E_L , J s^{-1}), the
 292 runoff energy when runoff leaves the plunge pool (E_H , J s^{-1}), and the runoff energy at the bottom of
 293 gully bed (E_B , J s^{-1}) were calculated as following. The calculation was consistent with the theory of
 294 minimum rate of energy dissipation expressed by Yang (1971a, 1971b).

$$295 E_T = \rho_w g q [(L_l + L_g) \tan \theta + H_h] \quad (9)$$

$$296 E_L = \rho_w g q [(L_m + L_g) \tan \theta + H_h] + \frac{1}{2} \rho_w q V_J^2 \quad (10)$$

$$297 E_H = \rho_w g q \left(L_m + L_g - V_b \sqrt{\frac{2h}{g}} \right) \tan \theta + \frac{1}{2} \rho_w q V_P^2 \quad (11)$$

298
$$E_B = \frac{1}{2} \rho_w q V_B^2 \quad (12)$$

299 where the L_l (m) and L_g (m) are the projection length of UA and GB, respectively, during gully
 300 head migration; L_m (m) is the gully head retreat distance; H_h (m) is the initial gully headcut height.
 301 V_P (m s^{-1}) and V_B (m s^{-1}) are the runoff velocity runoff leaving the plunge pool and GB, respectively.

302 —Therefore, the total runoff energy consumption (ΔE_T , J s^{-1}), the runoff energy consumption of
 303 UA (ΔE_L , J s^{-1}), the runoff energy consumption of GH (ΔE_H , J s^{-1}) and the runoff energy consumption
 304 of GB (ΔE_B , J s^{-1}) could be calculated as follows.

305
$$\Delta E_T = E_T - E_B \quad (13)$$

306
$$\Delta E_L = E_T - E_L \quad (14)$$

307
$$\Delta E_H = E_L - E_H \quad (15)$$

308
$$\Delta E_B = E_H - E_B \quad (16)$$

309 2.4.4 Statistical analysis

310 The curve regression analysis method was employed to determine the quantitative relations
 311 between hydraulic characteristics, jet properties, runoff energy consumption and soil erosion rate and
 312 inflow discharge. The fitted equations between soil loss rate of three landform units and hydraulic
 313 characteristics, jet properties, and energy consumption were also quantified by the curve regression.
 314 The soil erosion volume of upstream area, gully head and gully bed were derived from the DEM of
 315 different stages through the ArcGIS 10.0 software. The data analyse was executed by using SPSS
 316 software (version 6.0) and figure plotting was carried out with Origin 8.5 and PowerPoint 2016
 317 software.

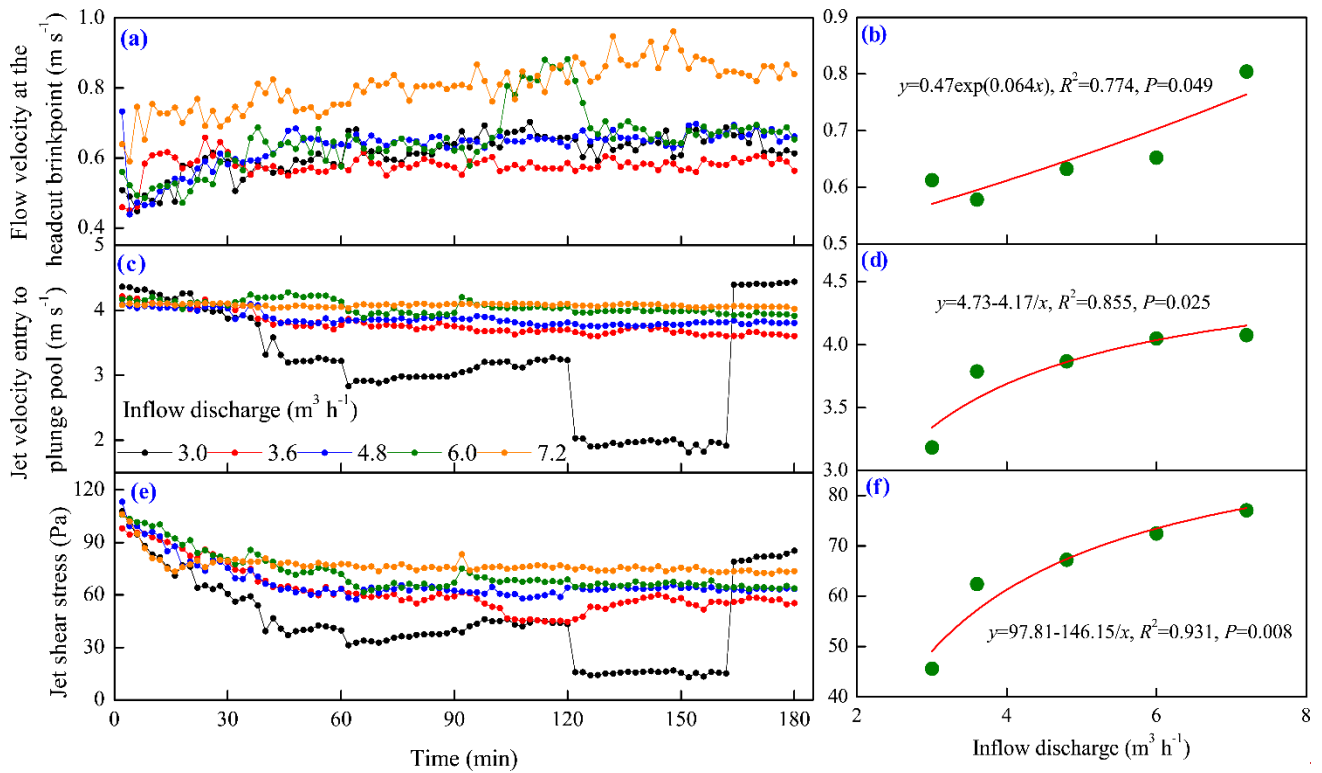
318 3 Results

319 3.1 Spatial-temporal changes in jet properties and runoff hydraulic

320 3.1.1 Jet properties of gully head

321 Fig. 4 shows the temporal change in the three jet property parameters of gully head (GH) under
 322 different inflow discharge conditions. Overall, the flow velocity at the headcut brinkpoint (V_b)
 323 increased obviously in the first 30 min and then showed a gradually stable tendency with some
 324 degree of fluctuation (Fig. 4a), and the fluctuation degree was enhanced by the increased inflow
 325 discharge. For example, the V_b increased sharply from 0.66 to 0.88 m s^{-1} during 100 — 124 min

326 under $6.0 \text{ m}^3 \text{ h}^{-1}$ inflow discharge due to the headwall failure near headcut enhancing the runoff
 327 turbulence. Regression analysis revealed the significant power relationships ($V_b = a \cdot t^b$, $R^2 = 0.139$ -
 328 0.704 , $P < 0.01$) between V_b and time (t) (Table 1). Furthermore, except for $3.6 \text{ m}^3 \text{ h}^{-1}$ condition, the
 329 a -value increased with the inflow discharge increased, but the b -value showed a weak variation (0.08
 330 $- 0.10$), indicating that the flow drainage from gully head can improve initial V_b but not change its
 331 change trend over time. The mean V_b exhibited a significantly exponential relationship with inflow
 332 discharge (Fig. 4b, $P < 0.05$). Contrary to the V_b , the jet velocity entry to plunge pool (V_e) and the jet
 333 shear stress (τ_j) experienced a gradually decreased trend with time (Fig. 4c, 4e). Notably, the V_e and
 334 τ_j suddenly decreased at 120th min and lasted nearly 40 minutes under $3.0 \text{ m}^3 \text{ h}^{-1}$ inflow discharge,
 335 which was mainly attributed to the developed second headcut shortening the jet-flow height. The
 336 temporal change of V_e could be described by logarithmic functions under $3.0 - 4.8 \text{ m}^3 \text{ h}^{-1}$ inflow
 337 discharges, and expressed by linear functions under the other inflow discharges, whereas the
 338 decrease of the τ_j with time could be presented by logarithmic functions under all inflow discharge
 339 conditions (Table 1). Furthermore, both of mean V_e and τ_j could be expressed by a positive “S”
 340 function of inflow discharge (Fig. 4d, 4f).



341

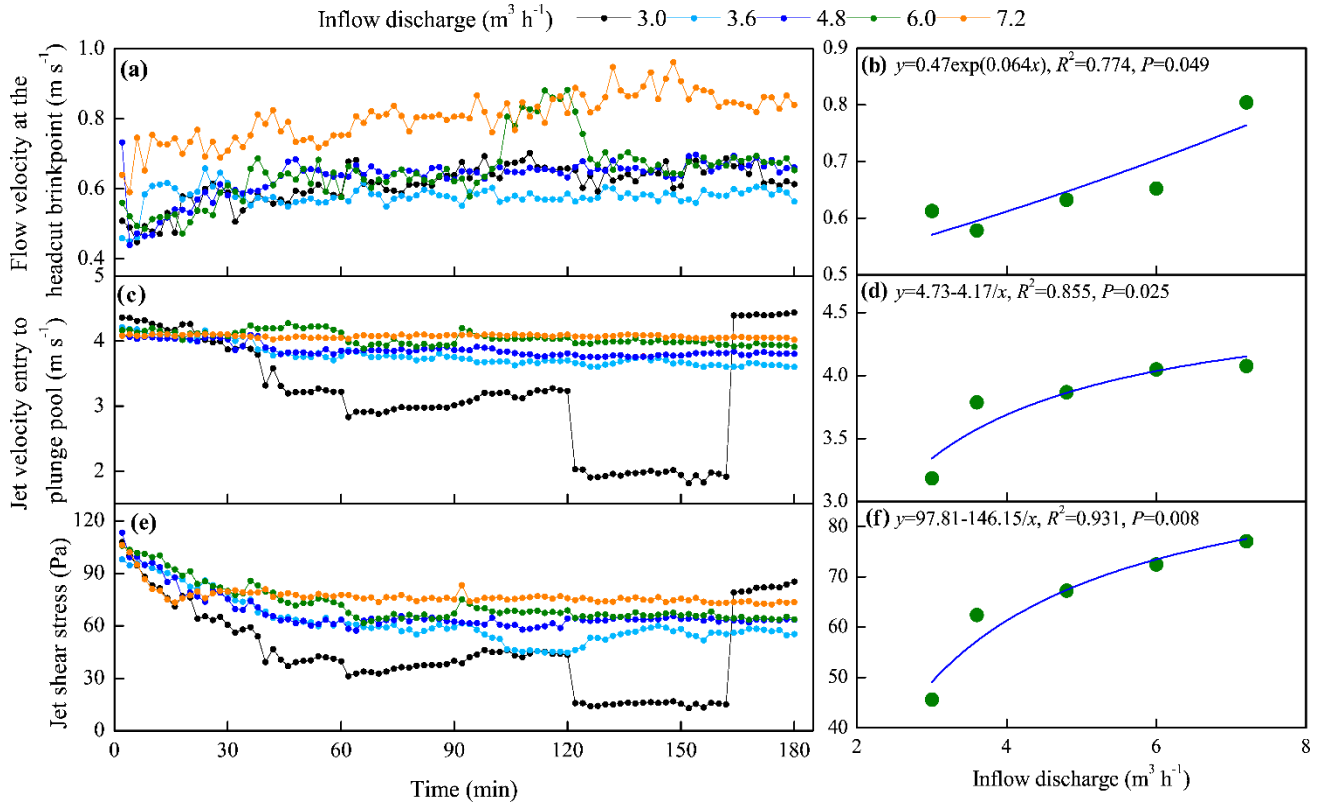


Figure 4. Temporal changes in jet properties of headcut and their relationships with inflow discharge.

Table 1. The relationships between jet properties of gully headcut and time.

Inflow discharge (m ³ h ⁻¹)	$V_b \sim t$	$V_e \sim t$	$\tau_j \sim t$
3.0	$V_b = 0.42 t^{0.09}$, $R^2 = 0.691^{**}$	$V_e = 5.28 - 0.49 \lg(t)$, $R^2 = 0.290^{**}$	$\tau_j = 110.86 - 15.44 \lg(t)$, $R^2 = 0.344^{**}$
3.6	$V_b = 0.53 t^{0.02}$, $R^2 = 0.139^{**}$	$V_e = 4.52 - 0.17 \lg(t)$, $R^2 = 0.859^{**}$	$\tau_j = 117.93 - 13.14 \lg(t)$, $R^2 = 0.823^{**}$
4.8	$V_b = 0.46 t^{0.08}$, $R^2 = 0.544^{**}$	$V_e = 4.25 - 0.09 \lg(t)$, $R^2 = 0.718^{**}$	$\tau_j = 109.22 - 9.93 \lg(t)$, $R^2 = 0.770^{**}$
6.0	$V_b = 0.52 t^{0.10}$, $R^2 = 0.509^{**}$	$V_e = 4.17 - 1.33 \times 10^{-3} t$, $R^2 = 0.478^{**}$	$\tau_j = 118.73 - 10.96 \lg(t)$, $R^2 = 0.876^{**}$
7.2	$V_b = 0.57 t^{0.08}$, $R^2 = 0.704^{**}$	$V_e = 4.09 - 1.38 \times 10^{-4} t$, $R^2 = 0.111^{**}$	$\tau_j = 95.68 - 4.42 \lg(t)$, $R^2 = 0.619^{**}$

Note: V_b , V_e and τ_j are runoff velocity at the headcut brinkpoint, runoff velocity entry to plunge pool and the jet shear stress, respectively. **** refers to the significance of 0.01.** The sample number is 90 for the fitted equations, and all fitted equations are at 0.01 significant level.

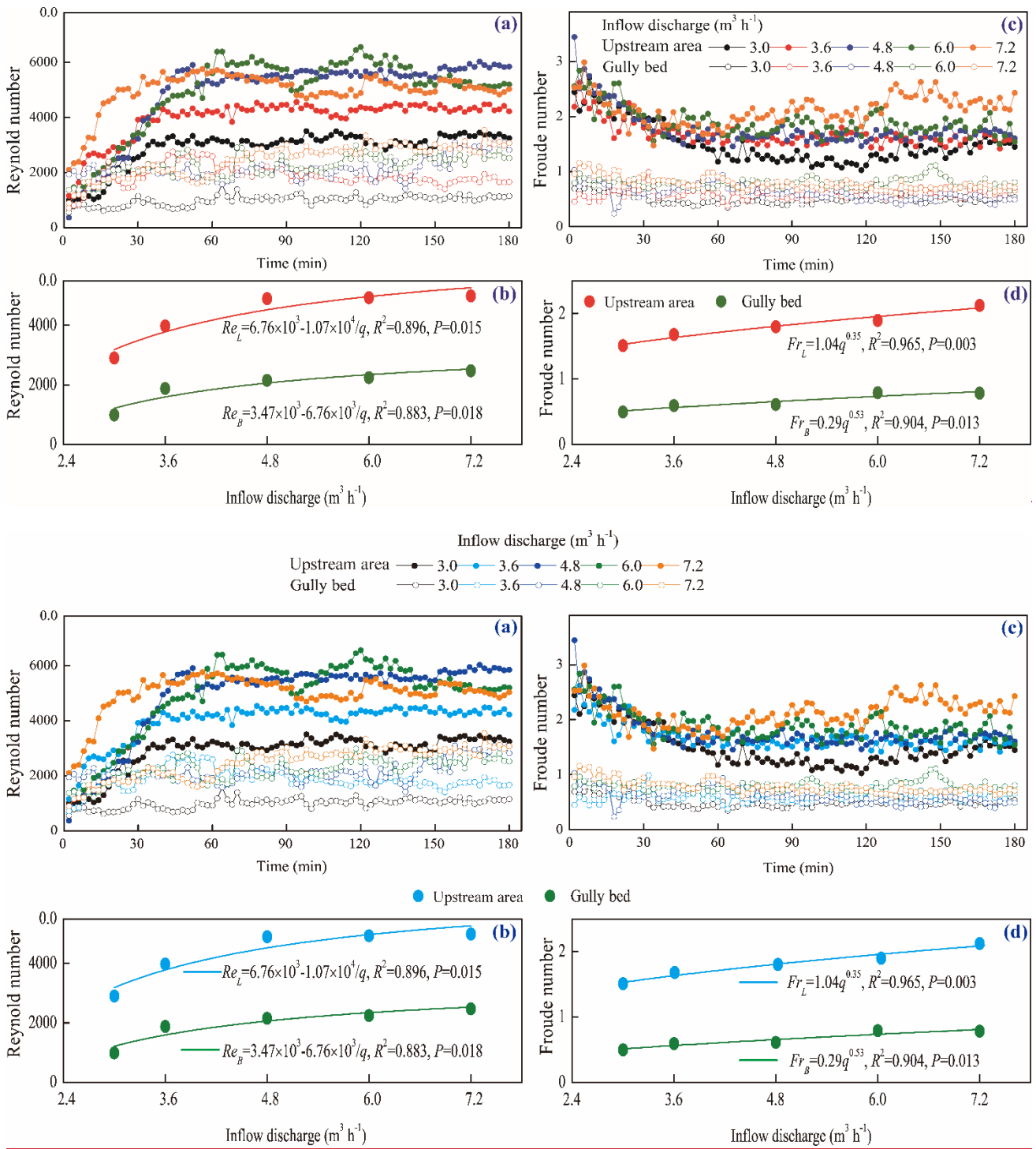
3.1.2 Runoff regime of upstream area and gully bed

The temporal changes in runoff Reynolds number (Re) and Froude number (Fr) of upstream area (UA) and gully bed (GB) and their relationships with inflow discharge are provided in Fig. 5. The Re of UA and GB showed a similar trend over time, that is, the Re firstly increased in the first 40 min

352 and then gradually stabilized (Fig. 5a). In addition, the Re of UA was larger than that of GB at any
353 time under same inflow discharge, indicating that the runoff turbulence became weaker after the
354 runoff of UA passed the gully head. The temporal variation in Re of UA could be described by
355 logarithmic and power functions, but, for the GB, the relationship was mainly dominated by power
356 function (Table 2). On average, the Re of GB was 50.5% - 65.9% less than that of UA, and the Re of
357 UA and GB both increased with the increase of inflow discharge as a power function (Fig. 5b).
358 However, as illustrated in Fig. 5c, the Fr experienced a completely opposite trend to Re . The Fr of
359 UA decreased in the first 60 min and then gradually stabilized, but the Fr of GB experienced a
360 relatively weak-fluctuating variation over time. For the most of cases, the change in Fr of UA and
361 GB over time could be expressed by logarithmic functions (Table 2). On average, the Fr of UA was
362 2.39 - 3.04 times that of GB for same inflow discharge, and the positive power function could
363 describe the relationship between Fr and inflow discharge (Fig. 5d).

364 Furthermore, the knowledge of open channel hydraulics is adopted to investigate the difference
365 in runoff regime between UA and GB. The specific definition is: the flow belongs to laminar when
366 Re is less than 500, the flow is turbulent when Re is larger than 2000, and the flow indicates
367 transitional when Re ranges from 500 to 2000; and $Fr = 1$ is the critical value for to distinguish the
368 subcritical and supercritical flow. The six flow regime zones were divided by three boundary lines
369 ($Re = 500$, $Re = 2000$, and $Fr = 1$) according to the logarithmic relationship between the flow
370 velocity and hydraulic radius (Fig. 6) (Xu et al., 2017b; Guo et al., 2020b). As shown, the runoff
371 regimes of UA and GB were located in five entirely different zones. The flow of UA was in the
372 supercritical-transition flow regime in the first 26 min and then gradually transformed to
373 supercritical-turbulent flow regime under 3.0 - 6.0 $\text{m}^3 \text{h}^{-1}$ inflow discharge, but the flow was
374 always in the supercritical-turbulent regime zone under 7.2 $\text{m}^3 \text{h}^{-1}$ inflow discharge. Moreover, the
375 higher inflow discharge would enhance the flow turbulent degree. The flow of GB belonged to
376 subcritical-laminar flow category in the initial 6 min, and then transformed to subcritical-transition
377 and subcritical-turbulent flow regime when inflow discharge was 3.0 and 3.6 $\text{m}^3 \text{h}^{-1}$. The flow was in
378 the subcritical-turbulent flow regime in most of experimental duration when the inflow discharge
379 was 4.8 - 7.2 $\text{m}^3 \text{h}^{-1}$. The difference in flow regime between UA and GB also indicated that the

380 presence of gully head can greatly reduce flow turbulence.



381

382

383 **Figure 5.** Temporal changes in runoff regime of upstream area and gully bed and their relationships with inflow
 384 discharge.

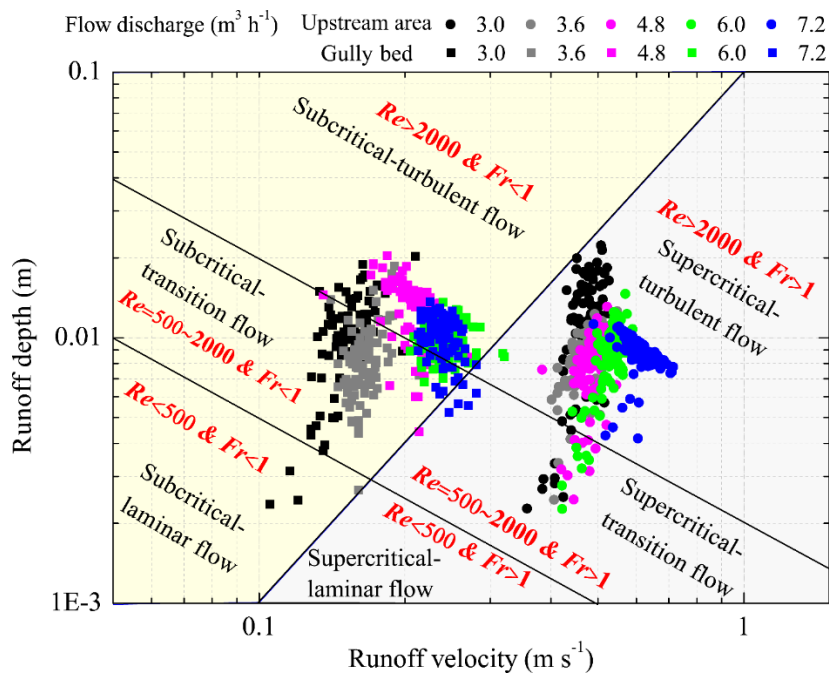
385

Table 2. Relationships between runoff hydraulic parameters and time.

Variable	Landfor m unit	Inflow discharge (m ³ h ⁻¹)				
		3.0	3.6	4.8	6.0	7.2
Reynold number	UA	$Re = 618.69 \lg(t) + 286.69$, $R^2 = 0.761^{**}$	$Re = 705.93 \lg(t) + 1006$, $R^2 = 0.815^{**}$	$Re = 1433 \lg(t) - 1159$, $R^2 = 0.849^{**}$	$Re = 946.64 t^{0.38}$, $R^2 = 0.794^{**}$	$Re = 2760 t^{0.14}$, $R^2 = 0.486^{**}$

	GB	$Re = 514.36 t^{0.15}$, $R^2 = 0.504^{**}$	—	$Re = 4.31 t + 1760$, $R^2 = 0.334^{**}$	$Re = 1.12 \times 10^3 t^{0.16}$, $R^2 = 0.566^{**}$	$Re = 744.99 t^{0.28}$, $R^2 = 0.872^{**}$
Froude number	UA	$Fr = 2.89 - 0.33 \lg(t)$, $R^2 = 0.651^{**}$	$Fr = 2.46 - 0.19 \lg(t)$, $R^2 = 0.651^{**}$	$Fr = 3.27 - 0.35 \lg(t)$, $R^2 = 0.656^{**}$	$Fr = 2.76 - 0.20 \lg(t)$, $R^2 = 0.515^{**}$	—
	GB	$Fr = 0.72 - 0.05 \lg(t)$, $R^2 = 0.326^{**}$	—	$Fr = 1.0 - 0.09 \lg(t)$, $R^2 = 0.359^{**}$	—	$Fr = 1.21 - 0.10 \lg(t)$, $R^2 = 0.634^{**}$
Shear stress	UA	$\tau = 0.66 \lg(t) + 0.55$, $R^2 = 0.737^{**}$	$\tau = 1.18 \lg(t) + 0.78$, $R^2 = 0.813^{**}$	$\tau = 1.32 \lg(t) - 0.62$, $R^2 = 0.817^{**}$	$\tau = 1.50 \lg(t) - 0.63$, $R^2 = 0.663^{**}$	$\tau = 1.11 \lg(t) + 0.99$, $R^2 = 0.819^{**}$
	GB	$\tau = 2.44 t^{0.08}$, $R^2 = 0.205^{**}$	$\tau = 3.88 t^{0.05}$, $R^2 = 0.106^{**}$	$\tau = 2.27 t^{0.19}$, $R^2 = 0.664^{**}$	$\tau = 3.64 t^{0.12}$, $R^2 = 0.212^{**}$	$\tau = 1.99 t^{0.27}$, $R^2 = 0.686^{**}$
Stream power	UA	$\omega = 0.34 \lg(t) + 0.16$, $R^2 = 0.761^{**}$	$\omega = 0.38 \lg(t) + 0.55$, $R^2 = 0.815^{**}$	$\omega = 0.78 \lg(t) - 0.63$, $R^2 = 0.849^{**}$	$\omega = 0.69 \lg(t) - 0.23$, $R^2 = 0.737^{**}$	$\omega = 0.27 \lg(t) + 1.56$, $R^2 = 0.436^{**}$
	GB	$\omega = 0.28 t^{0.15}$, $R^2 = 0.504^{**}$	$\omega = 0.69 t^{0.09}$, $R^2 = 0.123^{**}$	$\omega = 0.50 t^{0.19}$, $R^2 = 0.540^{**}$	$\omega = 0.83 t^{0.09}$, $R^2 = 0.338^{**}$	$\omega = 0.51 t^{0.23}$, $R^2 = 0.806^{**}$

Note: UA and GB refer to upstream area and gully bed. Re , Fr , τ and ω are Reynold number, Froude number, shear stress, stream power, respectively. **** refers to the significance of 0.01.** The sample number is 90 for the fitted equations, and the fitted equations are at 0.01 significant level.



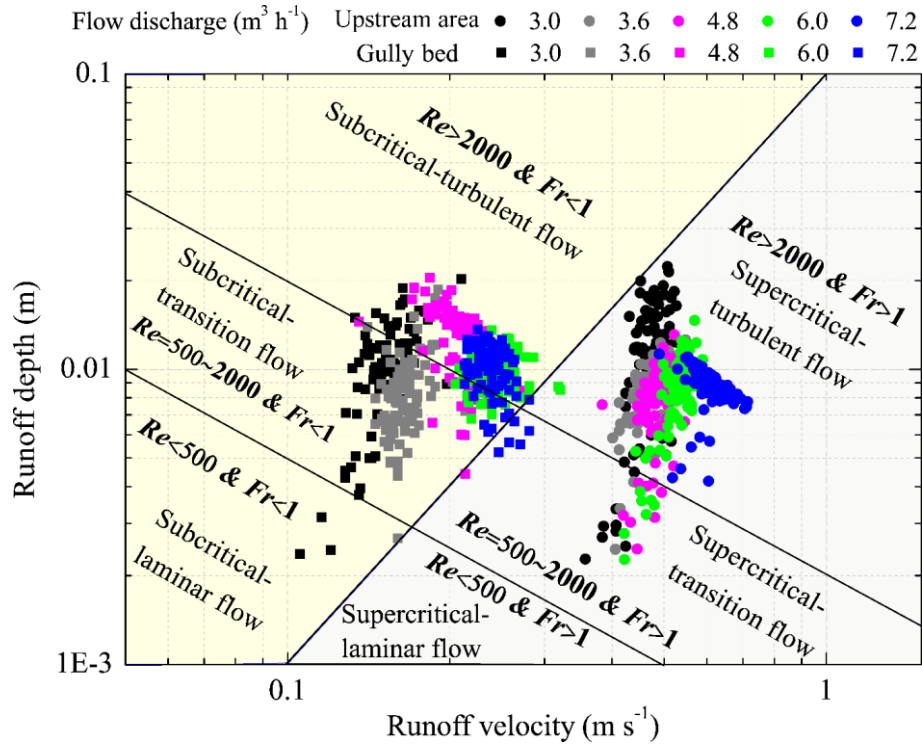


Figure 6. Runoff regime zones of upstream area and gully bed under different inflow discharge conditions.

3.1.3 Runoff shear stress and stream power of upstream area and gully bed

Fig.7 shows the temporal changes in runoff shear stress (τ) and stream power (ω) of upstream area (UA) and gully bed (GB) and their relationships with inflow discharge. Overall, the τ of UA and GB exhibited a gradually increased trend in the first 60 min, and whereafter, a relative steady state was obtained, but the larger inflow discharge perturbed the steady situation (Fig. 7a). Furthermore, the temporal change in τ of UA could be expressed by logarithmic functions, but the τ of GB showed a significant power function with experimental time (Table 2). On average, the τ of GB was 2.8% - 15.7% larger than the UA. The averaged τ of UA and GB increased with inflow discharge as a power function ($\tau = a - b/q$), and the GB had a faster increased-speed (b -value) than UA (Fig. 7b), signifying that the difference in τ between UA and GB would be widened with the inflow discharge increased. Similarly, the ω of UA and GB also exhibited a trend of gradual increase and stabilization (Fig. 7c). Different from the temporal change in τ , the ω of GB was always less than that of UA at any time for five inflow discharges. Likewise, the variation in ω of UA and GB over time exhibited a significant logarithmic and power function, respectively. On average, the ω of GB was 49.2% - 65.9% less than UA, and the positive increase in ω of UA and GB with inflow discharge could be expressed

by a power function (Fig. 7d).

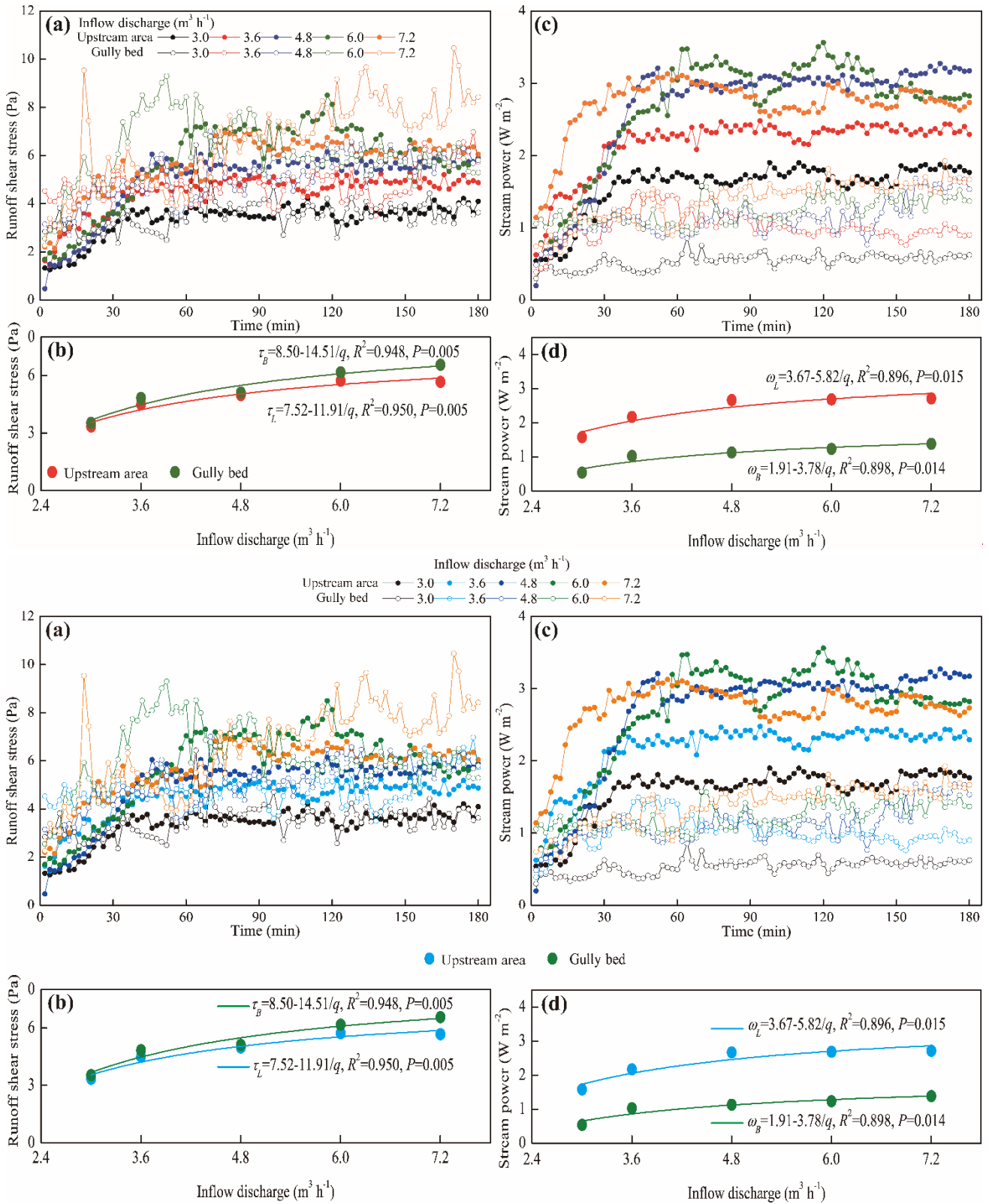


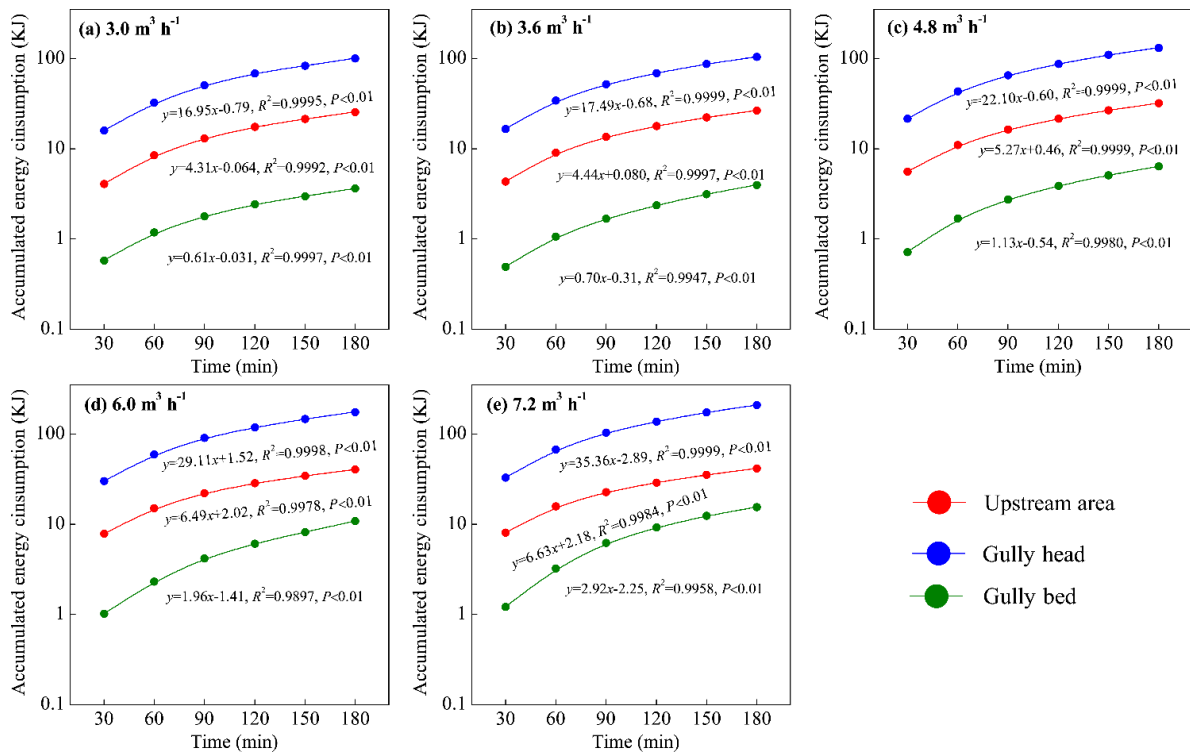
Figure 7. Temporal changes in runoff shear stress and stream power of upstream area and gully bed and their relationships with inflow discharge

412 3.2 Spatial-temporal change of energy consumption

413 Fig. 8 illustrates the temporal change in accumulated energy consumption of upstream area
414 (UA), gully head (GH) and gully bed (GB). The accumulated energy consumption of the three
415 landform units continued to linearly increase with time ($R^2=0.990-0.999$, $P<0.01$), of which the
416 accumulated energy consumption in GH was always the highest at any time, followed by UA and GB
417 under five inflow discharges. Moreover, the energy consumption rate (the slope-value of fitted
418 equation) in the three landform units is basically constant, indicating the spatial-temporal change in
419 energy consumption maintained a relatively steady state during gully headcut erosion. Moreover, the
420 energy consumption rate of GH was the highest, followed by UA and GB, and the energy
421 consumption rate in the three landform units also increased with the increase of inflow discharge.

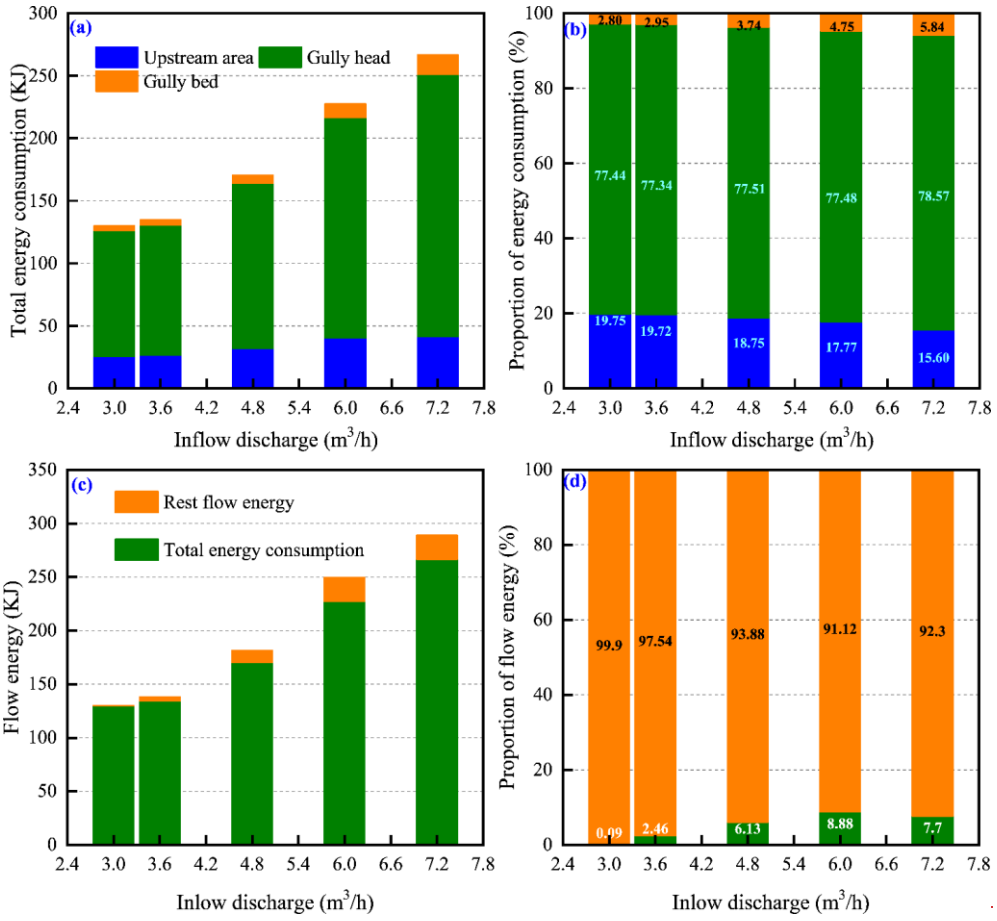
422 The variations of total energy consumption of UA, GH and GB and their proportions with
423 inflow discharge are shown in Fig. 9. As illustrated in Fig. 9a, both of the total energy consumption
424 of the “UA-GH-GB” system and the three landform units increased with the increase of inflow
425 discharge. When inflow discharge increased from 3.0 to 7.2 m³ h⁻¹, the total energy consumption of
426 the system, UA, GH and GB increased by 3.6% - 105.3%, 3.4% - 62.0%, 3.5% - 108.2% and 9.0% -
427 327.5%, respectively. Regression analysis revealed that the energy consumption of the system and
428 the three landform units increased with inflow discharge as an exponential function ($y=a\cdot\exp(b\cdot x)$,
429 $a=1.14-55.41$, $b=0.13-0.36$, $R^2=0.954-0.992$, $P<0.05$). Furthermore, in view of the proportion
430 of energy consumption, the energy consumption of UA accounted for 15.6% - 19.8% of total energy
431 consumption, and linearly decreased with inflow discharge increased ($R^2=0.933$, $P<0.05$), whereas
432 the proportion in GB (2.8% - 5.8%) linearly increased with inflow discharge increased ($R^2=0.983$,
433 $P<0.05$). However, the proportion of energy consumption (77.3% - 78.6%) in GH showed a weak
434 change with inflow discharge (Fig. 9b), signifying that the most of runoff energy (77.5% on average)
435 was consumed in the gully head position during headcut migration. Furthermore, we found that the
436 total energy consumption (129.89 - 266.60 KJ) under different flow discharge conditions accounted
437 for the 91.12% - 99.90% of total flow energy (Fig. 9c, 9d), which also indicated that only 0.10% -
438 8.88% of total flow energy remained at the outlet of the “UA-GH-GB” system. These results fully
439 implied that the most of flow energy (>91.12%) upstream from gully heads would be consumed

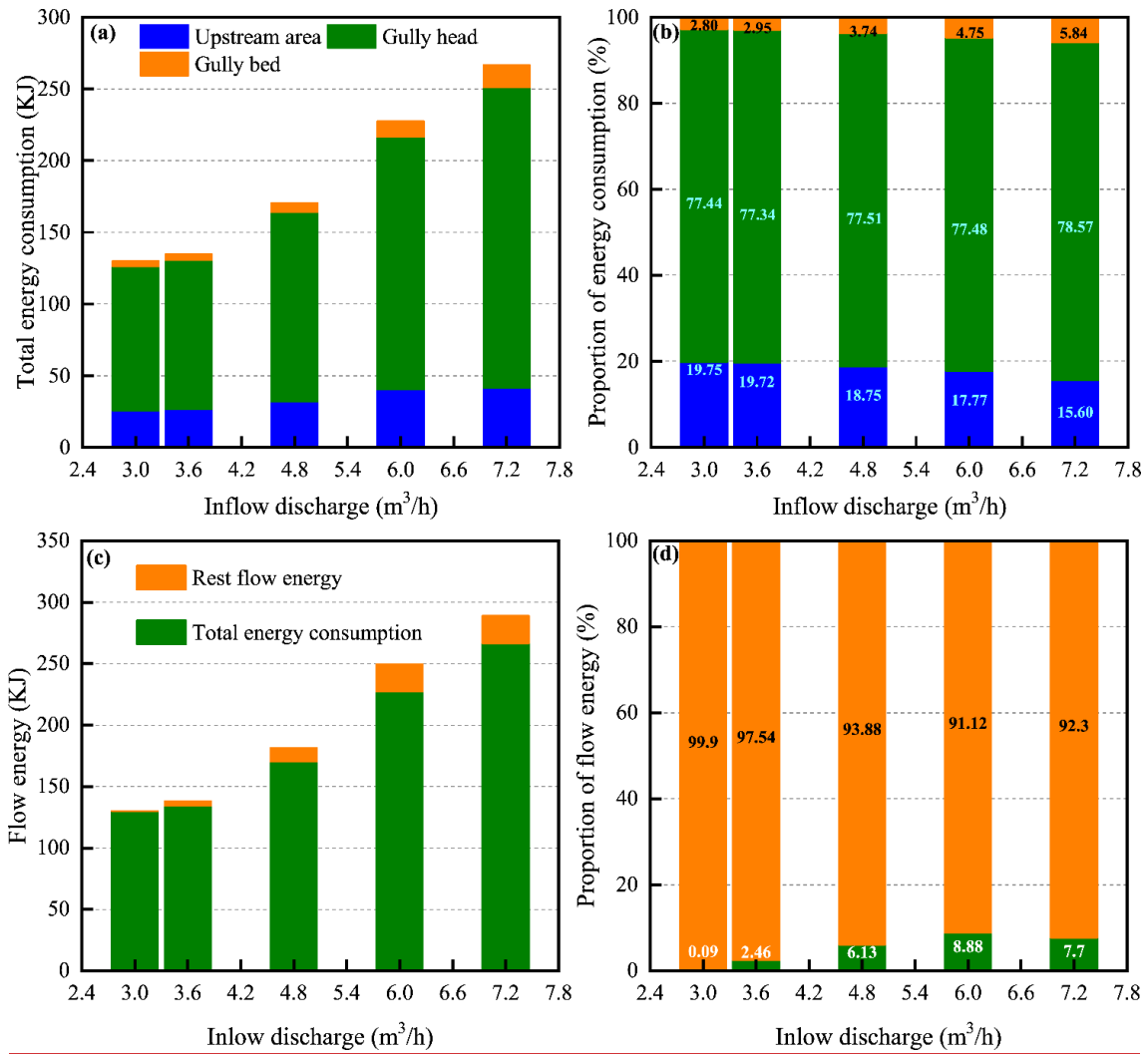
440 during gully erosion, of which the gully headcut erosion (including plunge pool erosion) is the main
 441 process consuming flow energy.



442
 443
 444

Figure 8. Temporal changes in runoff energy consumption of upstream area, gully head and gully bed under different inflow discharge conditions





446
447 **Figure 9.** Total he variation in energy consumption (a) and their proportions (b) of upstream area, gully head and
448 gully bed, and the total energy consumption and rest flow energy (c) and their proportions (d) with under different
449 inflow discharge conditions

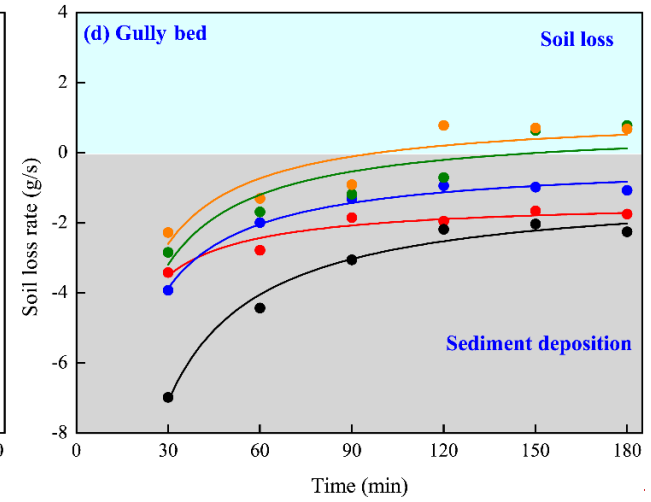
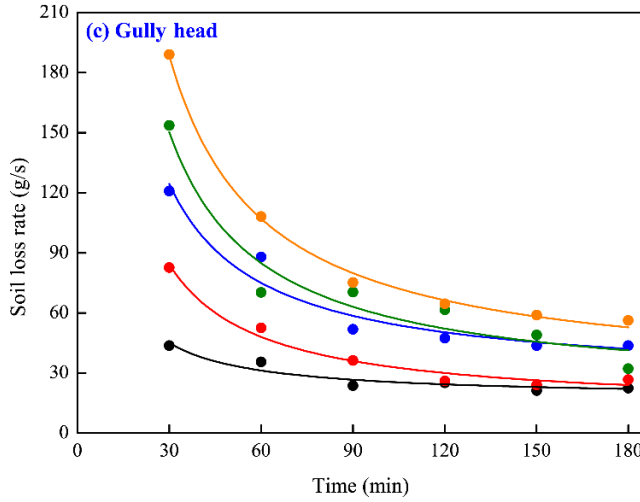
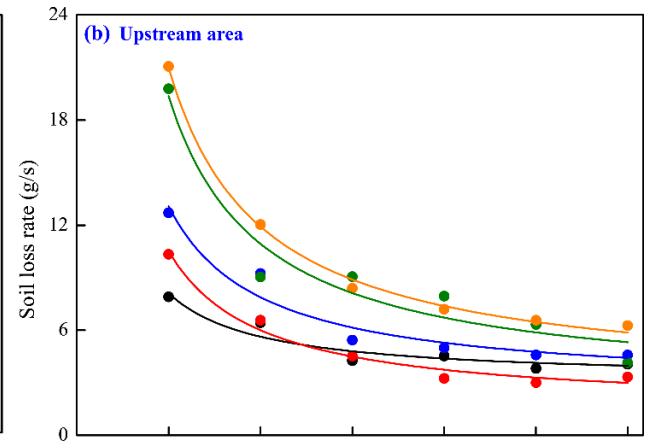
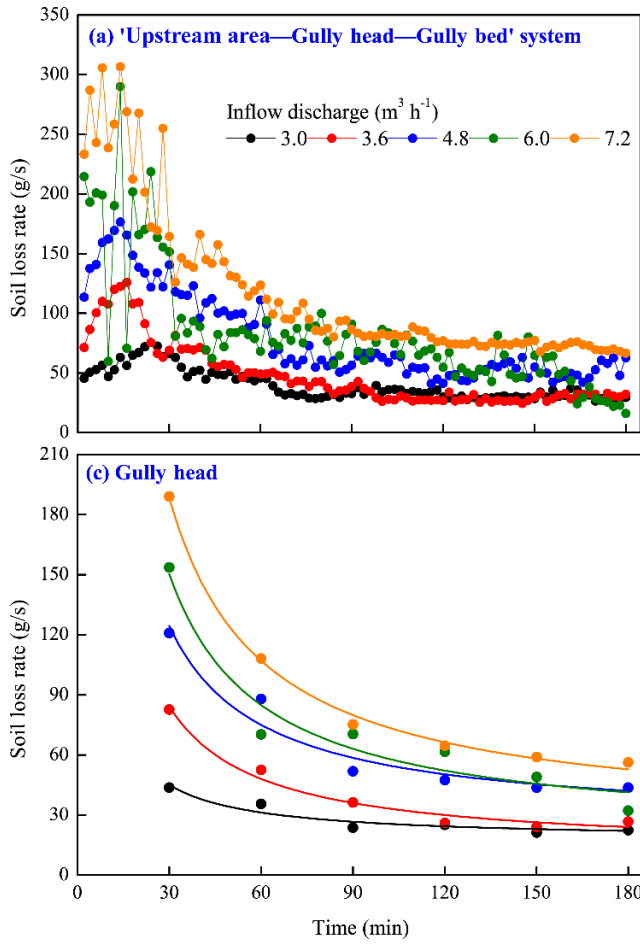
450 3.3 Spatial-temporal change of soil loss

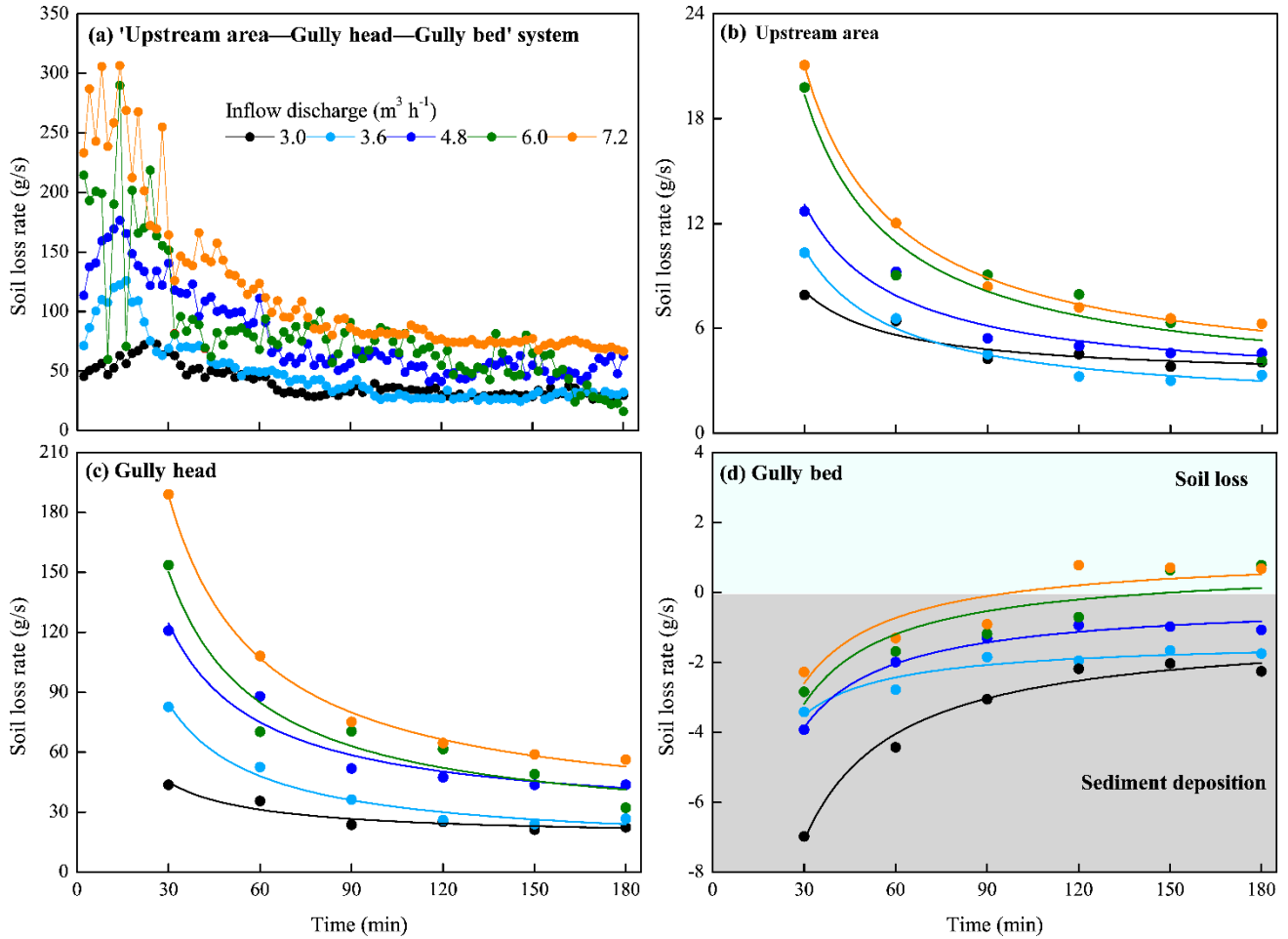
451 3.3.1 Soil loss process

452 Fig. 10a shows that the soil loss rate of the “upstream area (UA)—gully head (GH)—gully
453 bed (GB)” system rose to a peak in first 20 min, then gradually descend and levelled off. Especially
454 for the 6.0 and 7.2 m³ h⁻¹, the soil loss rate showed a severe fluctuation trend in the first 30 min. The
455 peak soil loss rate increased from 75.4 to 306.9 g s⁻¹ with increasing inflow discharge. The soil loss
456 of UA and GH experienced a similar change process. The soil loss rate was the highest in the early
457 stage of the experiment, and gradually decreased with time, and became stable after 120 min (Fig.
458 10b, 10c). Furthermore, the temporal variation in soil loss of UA and GH could be well expressed by

459 logarithmic function ($S_L = a - b \cdot \ln(t)$, $P < 0.05$, Table 3), and the a -value (representing initial soil loss
460 rate) and b -value (reflecting the reduction rate of soil loss rate with time) increased with increasing
461 inflow discharge, indicating that larger inflow discharge can improve initial soil loss of UA and GH
462 and also expedite the decrease of soil loss rate.

463 However, the GB presented a completely different soil loss process from UA and GH (Fig. 10d).
464 The GB was always characterized by sediment deposition during the whole experiment for the 3.0 –
465 – 4.8 $\text{m}^3 \text{h}^{-1}$ inflow discharges. The sediment deposition rate gradually decreased with time and
466 presented a significant “S” function over time ($S_B = a/t - b$, $R^2 = 0.918 - 0.982$, $P < 0.01$, Table 3).
467 When the inflow discharge was larger than 4.8 $\text{m}^3 \text{h}^{-1}$, the sediment generated from UA and GH was
468 deposited firstly in the GB and then gradually transported, and the temporal change of deposited
469 sediment on GB accorded with logarithmic functions ($R^2 = 0.936$ and 0.906 , $P < 0.01$, Table 3).
470 Furthermore, two critical time points (135 min and 111 min) can be derived from the two fitted
471 logarithmic equations, which distinguished sediment deposition from sediment transport, signifying
472 that the runoff began to transport the deposited sediment on GB after 135 min and 111 min for 6.0
473 and 7.2 $\text{m}^3 \text{h}^{-1}$ inflow discharges.





475

476 **Figure 10.** Temporal variation in soil loss rate of the “upstream area—gully head—gully bed” system (a), upstream
 477 area (b), gully head (c) and gully bed (d) each landform unit

478

Table 3. Relationships between soil loss rate of three landform units and time

Inflow discharge (m ³ h ⁻¹)	Fitted equations		
	Upstream area	Gully head	Gully bed
3.0	$S_L = 15.71 - 2.34 \ln(t), R^2 = 0.909^{**}$	$S_H = 87.12 - 12.99 \ln(t), R^2 = 0.908^{**}$	$S_B = -182.62/t - 1.01, R^2 = 0.980^{**}$
3.6	$S_L = 23.97 - 4.18 \ln(t), R^2 = 0.938^{**}$	$S_H = 191.82 - 33.44 \ln(t), R^2 = 0.939^{**}$	$S_B = -64.46/t - 1.36, R^2 = 0.918^{**}$
4.8	$S_L = 28.76 - 4.85 \ln(t), R^2 = 0.930^{**}$	$S_H = 273.64 - 46.17 \ln(t), R^2 = 0.929^{**}$	$S_B = -109.36/t - 0.22, R^2 = 0.982^{**}$
6.0	$S_L = 44.0 - 7.69 \ln(t), R^2 = 0.884^*$	$S_H = 341.59 - 59.74 \ln(t), R^2 = 0.885^*$	$S_B = 2.03 \ln(t) - 9.96, R^2 = 0.936^{**}$
7.2	$S_L = 47.34 - 8.25 \ln(t), R^2 = 0.922^{**}$	$S_H = 425.24 - 74.07 \ln(t), R^2 = 0.924^{**}$	$S_B = 1.86 \ln(t) - 8.76, R^2 = 0.906^{**}$

479

Note: S_L , S_H and S_B are the soil loss rate of upstream area, gully head and gully bed, respectively. The sample No. is
 480 6 for fitting equation. * and ** indicate the significant level of 0.05 and 0.01.

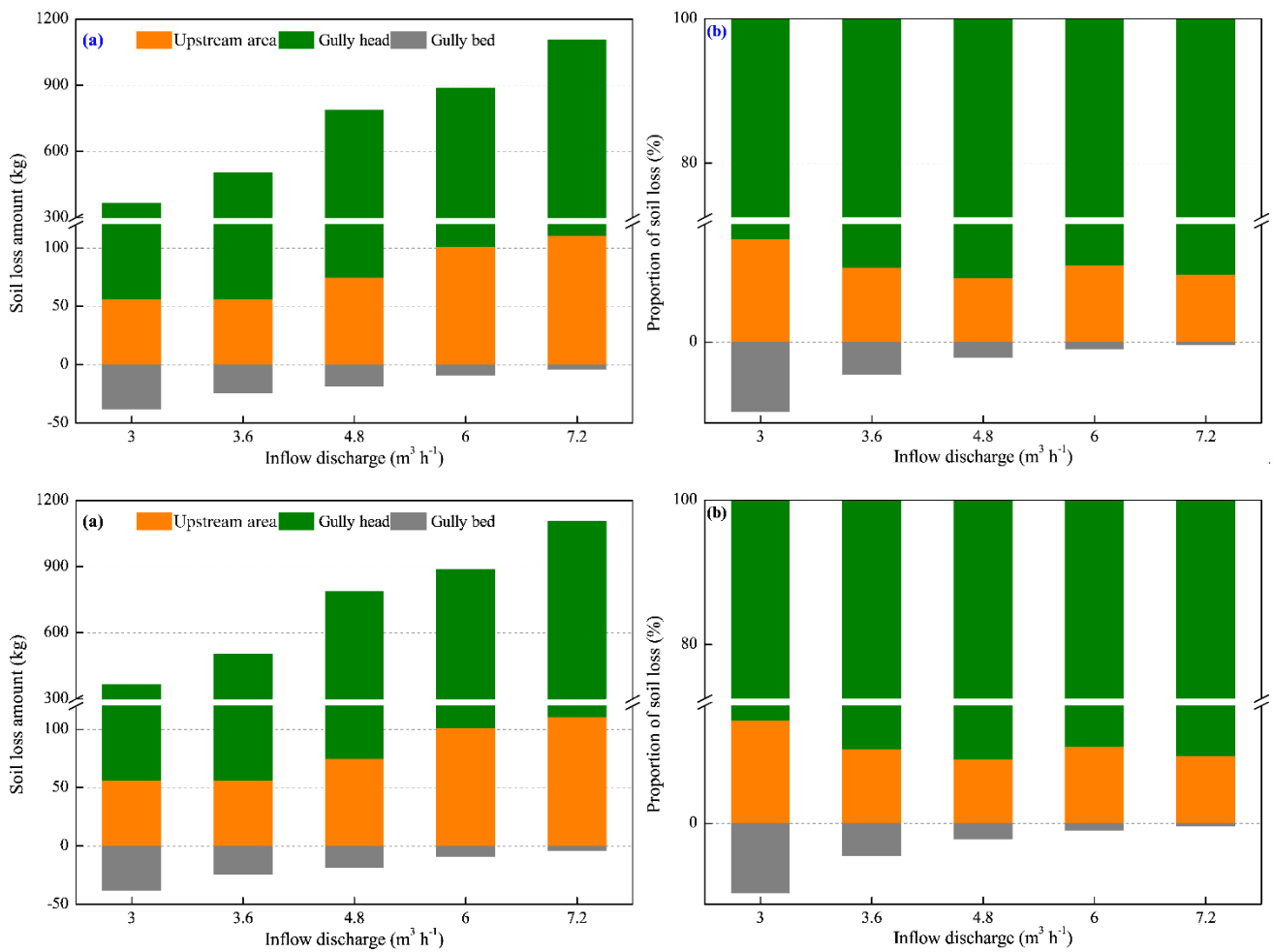
481

3.3.2 Spatial distribution of soil loss

482

The variation in soil loss amount and proportion of the three landform units (UA, GH, GB) with
 483 inflow discharge is shown in Fig. 11. As illustrated in Fig. 11a, for the experiments of five inflow
 484 discharges, the soil loss was dominant in the UA and GH, but the GB was dominated by sediment

485 deposition due to the weaker sediment transport capacity of runoff on GB than sediment
 486 deliverability of UA and GH. Furthermore, the soil loss amount of UA and GH ranged from 55.9 to
 487 110.7 kg and from 310.0 to 994.8 kg, respectively, and increased linearly with increasing inflow
 488 discharge ($R^2=0.966$ and 0.969 , $P<0.05$). The sediment deposition amount of GB ranged from 4.2 to
 489 37.7 kg, and decreased with inflow discharge as a logarithmic function ($R^2=0.961$, $P<0.05$). In
 490 terms of proportion of soil loss (Fig. 11b), the proportion of UA and GH reached the maximum
 491 (15.3%) and minimum (84.7%), respectively under $3.0 \text{ m}^3 \text{ h}^{-1}$ inflow discharge, whereas, the
 492 proportion exhibited a little change (UA: 9.5% - 11.4%; GH: 88.6% - 90.5%) when the inflow
 493 discharge is $7.2 \text{ m}^3 \text{ h}^{-1}$. Remarkably, the proportion of deposited sediment amount on GB to total soil
 494 loss amount ranged from 0.4% to 10.3%, and decreased exponentially with inflow discharge ($R^2=$
 495 0.992 , $P<0.001$).



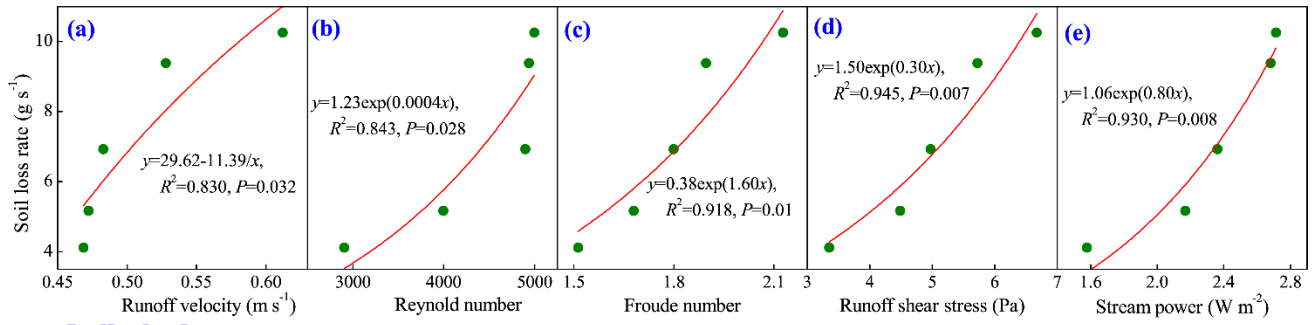
496
 497
 498 **Figure 11.** Variation in soil loss amount (a) and proportion (b) of upstream area, gully head and gully bed with
 499 inflow discharge

500 3.4 Spatial change in hydrodynamic mechanism of soil loss

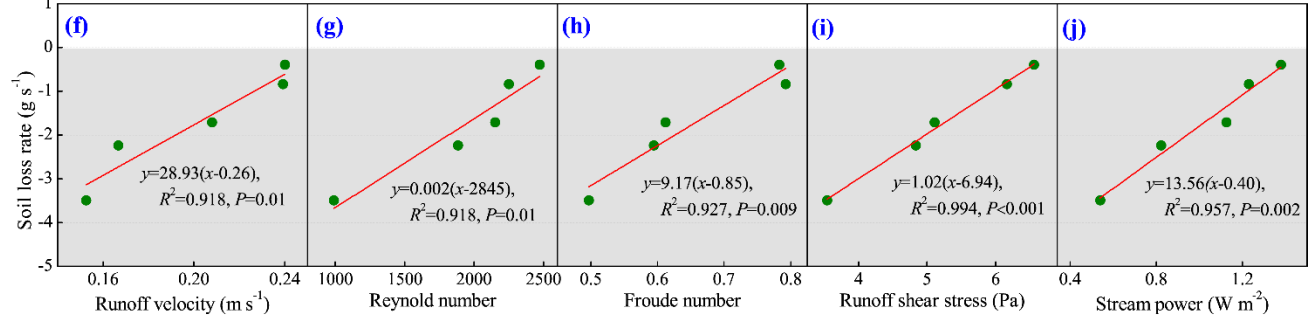
501 3.4.1 Relationships between soil loss and hydraulic parameters

502 Fig. 12 indicates the significant difference in the relationships between soil loss rate and
503 hydraulic parameters among the three landform units (Fig. 12). For the upstream area (UA), the soil
504 loss rate could be described as a series of exponential functions of runoff velocity, Reynold number,
505 Froude number, runoff shear stress and stream power, of which the runoff shear stress and stream
506 power had a closer correlation with soil loss (Fig. 12a - 12e, $R^2 = 0.830 - 0.945$). Furthermore, the
507 increased speed of soil loss rate obviously increased with the increasing hydraulic parameters (except
508 for runoff velocity), indicating that soil loss of UA showed a stronger sensitive response to increasing
509 hydraulic properties. However, the soil loss rate of gully bed (GB) linearly increased with the
510 above-mentioned five parameters (Fig. 12f - 12j, $R^2 = 0.918 - 0.994$), which suggested that the
511 decreased rate of sediment deposition of GB is basically constant with the increasing hydraulic
512 properties. Further analysis showed that the critical runoff velocity, Reynold number, Froude number,
513 runoff shear stress and stream power for triggering the transformation of sediment deposition to soil
514 erosion on GB, and the critical values are 0.26 m s^{-1} , 2845, 0.85, 6.94 Pa and 0.40 W m^{-2} ,
515 respectively. For the gully head (GH) position, the soil loss was significantly affected by jet velocity
516 entry to plunge pool and jet shear stress (Fig. 12l and 12m, $R^2 = 0.862$ and 0.939), while the
517 relationship between soil loss and flow velocity at the headcut brink-point was not significant (Fig.
518 12k, $P = 0.065$).

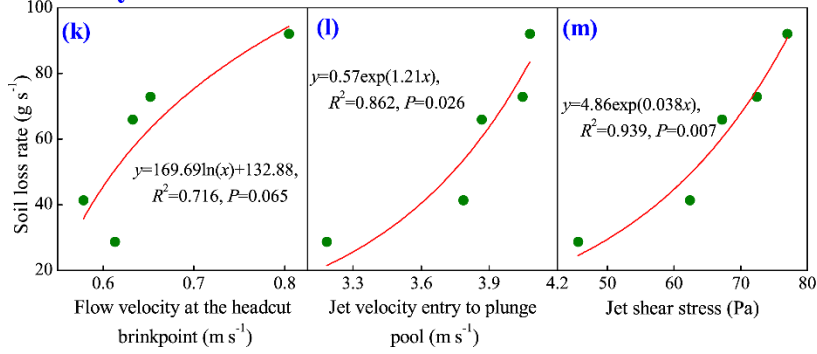
Upstream area



Gully bed



Gully head



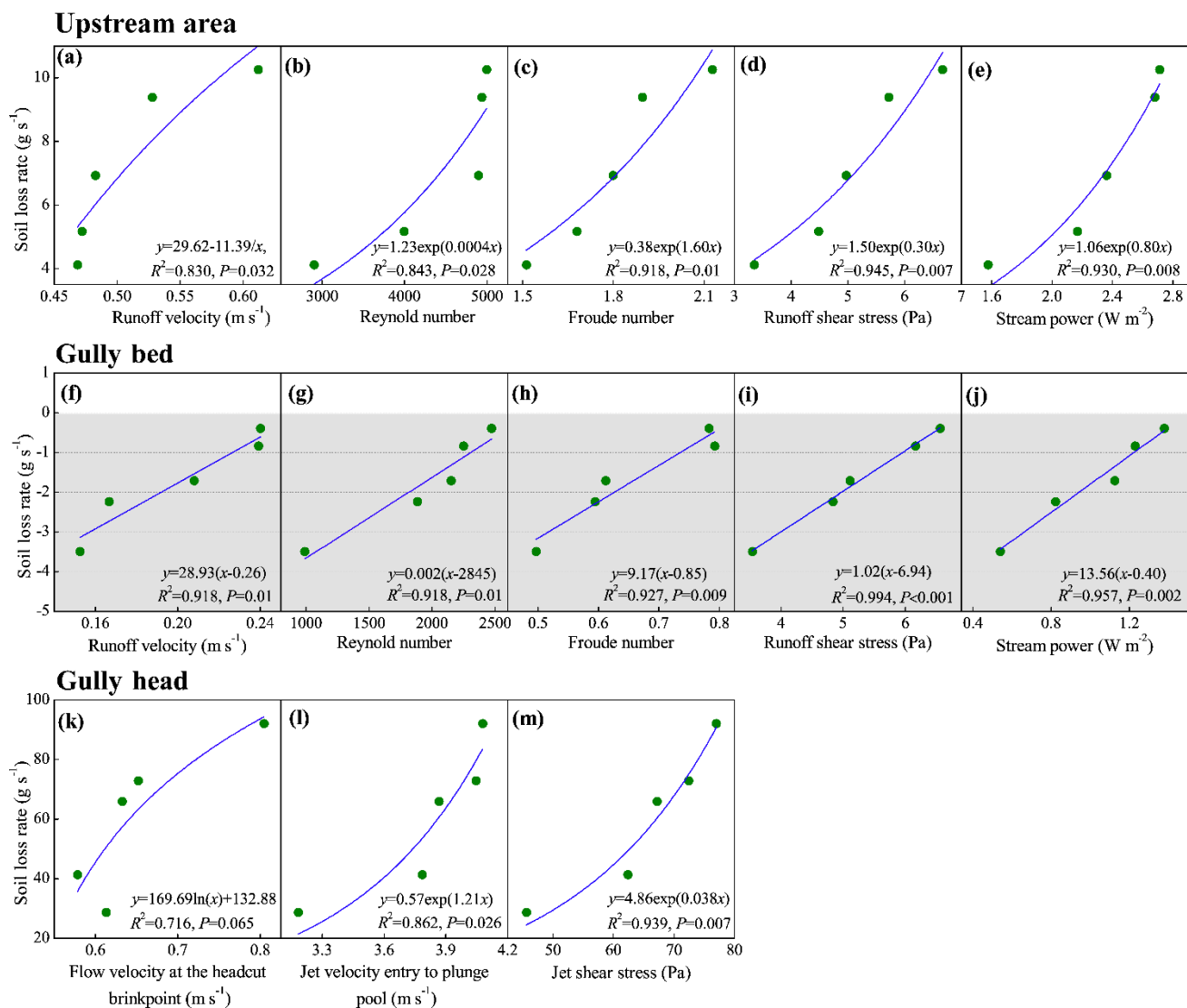


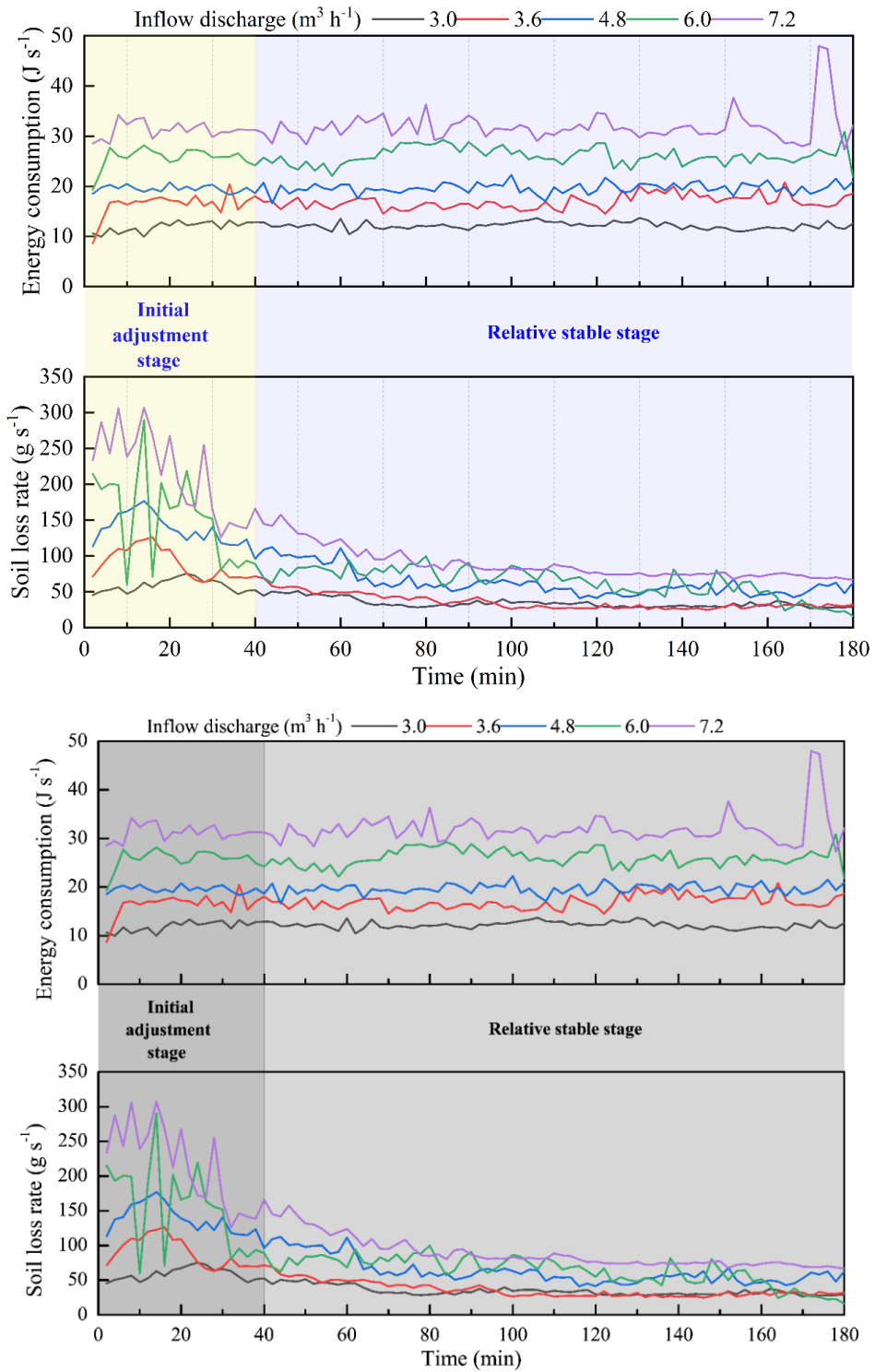
Figure 12. Relationships between soil loss rate of upstream area, gully bed and gully head three landform units and runoff hydraulic and jet properties

3.4.2 Response of soil loss to energy consumption

The synchronous change of soil loss of “UA-GH-GB” system and total energy consumption can be divided into two stages (Fig. 13). In the initial adjustment stage (0_ - 40 min), the topsoil layer of UA had the relative higher erodibility and was the main resource of soil loss, which caused the relative lower flow velocity at the brinkpoint of gully head. Therefore, the most of flow discharge was transformed as on-wall flow, so the most of flow energy consumed at the headwall. So, in this stage, UA and gully headwall are the main positions of soil loss, and the most of flow energy was also consumed in the two positions. With the gradual adjustment of upstream area morphology, the gully erosion process entered into the relative stable stage (40_ - 180 min). In this stage, the flow

533 velocity at headcut obviously increased and showed a slight change (Fig. 4a), and thus the headwall
534 erosion and plunge pool erosion also experienced a relative stable process. As a result, the soil loss
535 and flow energy consumption exhibited a similar change process. Occasionally, the occurrence of
536 several gully head and bank collapse events altered the synchronous change process of soil loss and
537 energy consumption.

538 As illustrated in Fig. 14, on average, the soil loss rate of the “UA-GH-GB” system and the three
539 individual landform units was positively and significantly related to the energy consumption
540 ($P < 0.05$), and a logarithmic function was found to fit the relationship between soil loss rate and
541 energy consumption best ($R^2 = 0.889 - 0.987$). The critical energy consumption initiating the system
542 is 7.53 J s^{-1} (Fig. 14a). Furthermore, there is critical energy consumption to initiate soil erosion of the
543 upstream area (UA) and gully head (GH) based on the fitted logarithmic functions (Fig. 14b, 14c).
544 The critical energy consumption for GH (5.79 J s^{-1}) is 2.57 times greater than that (1.62 J s^{-1}) of the
545 UA. Similarly, for the gully bed (Fig. 14d), the minimum energy consumption (1.64 J s^{-1}) is needed
546 to trigger the transformation of sediment deposition to soil loss. We found that the sum of critical
547 energy consumption initiating three landform units (9.05 J s^{-1}) was larger than the critical value
548 initiating the system, which was mainly attributed to the mass failure of gully head and bank
549 inputting the additional potential energy into the flow.



550

551

552

553

Figure 13. Synchronous change of soil loss rate of “upstream area-gully head-gully bed” system and total energy dissipation during headcut erosion

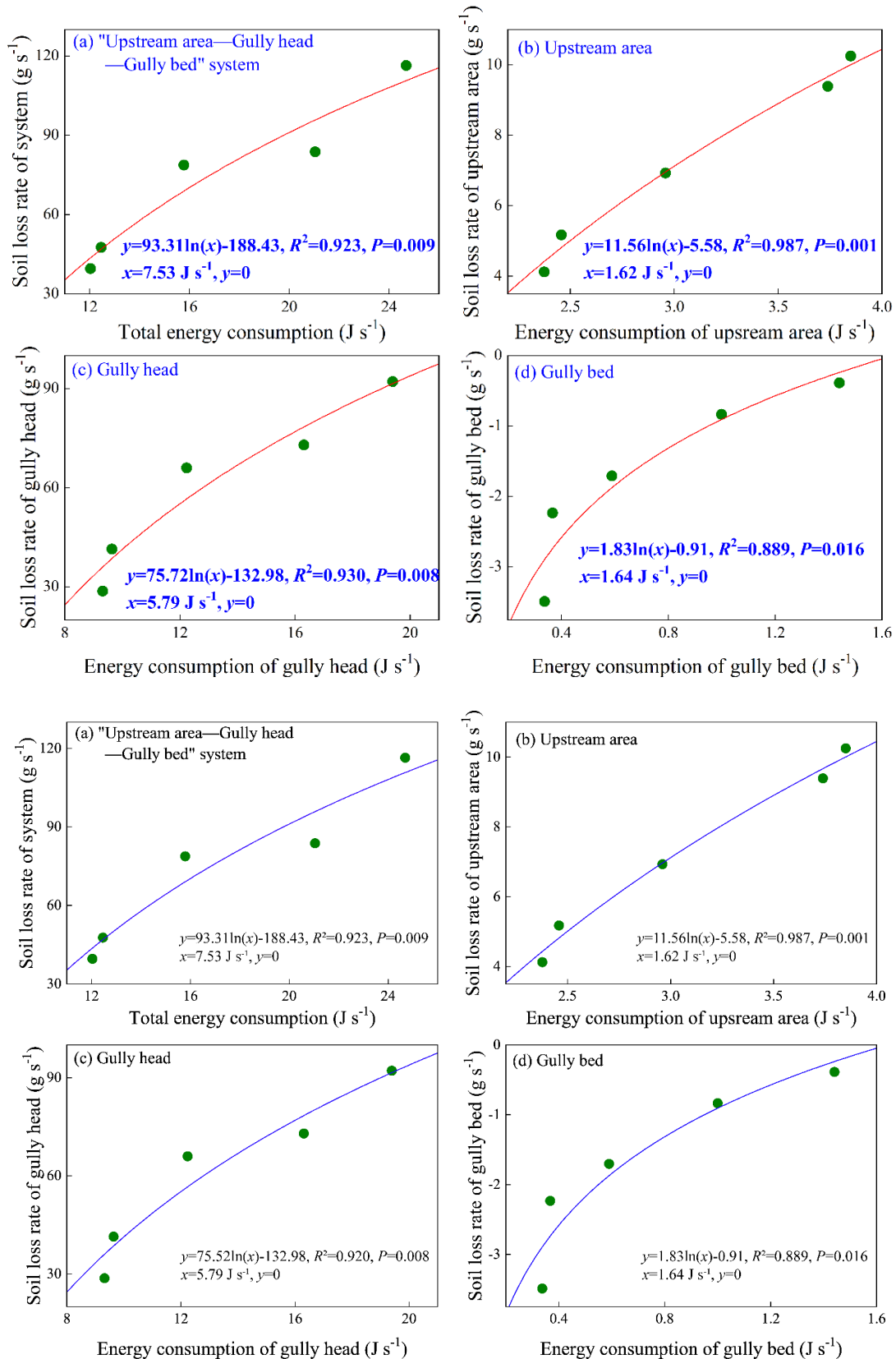


Figure 14. Relationships between soil loss rate of “upstream area-gully head-gully bed” system (a), upstream area (b), gully head (c) and gully bed(d) and three individual landform units and energy consumption

559 4 Discussion

560 4.1 Spatial-temporal changes in hydraulic properties

561 This study showed that the runoff velocity at the headcut brink-point (V_b) firstly raised and then
562 gradually stabilized with experimental duration (Fig. 4a), which was closely corresponded to the
563 gradually decreased runoff width on the upstream area over time (Shi et al., 2020a). However, this
564 result was inconsistent with Zhang et al (2016, 2018) and Shi et al (2020b) who reported that the V_b
565 decreased over time, which was mainly due to the gradually increased roughness and resistance of
566 underlying surface over time reducing the runoff velocity in their studies (Battany and Grismer, 2015;
567 Su et al., 2015). The further analysis of power function between V_b and time ($V_b = a \cdot t^b$, Table 1)
568 showed that the a -value increased but the b -value showed a weak variation with the inflow discharge
569 increased, indicating that upstream flow discharge can improve initial V_b but not affect its change
570 trend over time. Therefore, we can extrapolate the erosion process and rule of upstream area from
571 this simulation test to the actual ground situation. By contrast, the jet velocity entry to plunge pool
572 (V_e) and jet shear stress (τ_j) experienced a gradually decreased process (Fig. 4c, 4e), which was
573 mainly attributed to the fact that the development of several second-headcut steps caused more
574 energy consumption in plunge pools and the lower potential energy at headcut brink-point due to the
575 shortened jet flow height (Guo et al., 2019; Jiang et al., 2020). This result, however, differed from the
576 finding of Zhang et al. (2016) who stated the V_e and τ_j remained stable as the experiments progressed,
577 which was mainly attributed to the weak change of jet-flow height induced by slow headcut retreat.
578 This comparison manifested that the jet flow properties was strongly determined by the headcut
579 retreat process.

580 For the runoff hydraulic of upstream area (UA) and gully bed (GB), the Reynold number Re of
581 UA and GB initially increased and gradually stabilized, but the Froude number Fr showed an
582 opposite trend. This phenomenon was agreed with previous studies (e.g., Su et al., 2015; Zhang et al.,
583 2016). Besides, the Re and Fr of UA were larger than that of GB by 50.5% - 65.9% and 1.39 - 2.04
584 times, respectively, under same inflow discharge upstream gully head, indicating that the runoff
585 turbulence became weaker after the runoff of UA passed the gully head and experienced plunge pool
586 erosion (Shi et al., 2020a). More evidently, the runoff on UA was in the supercritical-transition and

587 supercritical-turbulent flow regime ($Re > 500$, $Fr > 1$), whereas the runoff on GB belonged to
588 subcritical-transition and subcritical-turbulent flow regime ($Re > 500$, $Fr < 1$). However, Su et al.
589 (2015) found that the steady state Re of gully bed was higher than that of upstream area, which was
590 mainly attributed to the difference in slope gradient. In their study, the larger gully bed slope gradient
591 than upstream area would accelerate the runoff velocity and thus enhance flow turbulence (Bennett,
592 1999; Pan et al., 2016). Furthermore, compared to UA, the τ and ω of GB increased and decreased
593 by 2.8% - 15.7% and 49.2% - 65.9%, respectively. The increased shear stress was caused by the
594 decrease of flow velocity on gully bed, and the drastically decreased stream power can reflect the
595 energy consumption of flow for transporting sediment on gully bed. This result was different from
596 some previous experimental studies on gully and bank gully under different conditions. Previous
597 studies have proven that the lots of factors including plunge pool size, slope gradient, initial step
598 height, and soil texture influenced the hydraulic properties from upstream area to gully bed is
599 affected by various factors (Bennett and Casali, 2001; Wells et al., 2009a, 2009b).

600 **4.2 Spatial-temporal change in runoff energy consumption and soil erosion**

601 Our study revealed that the accumulated runoff energy consumption of the upstream area (UA),
602 gully headcut (GH) and gully bed (GB) linearly increased over time (Fig. 8), indicating the
603 spatial-temporal change in energy consumption maintained a relatively steady state during gully
604 headcut erosion. However, the flow energy consumption of bank gully in three landform units
605 logarithmically increased over time (Su et al., 2015). This difference further manifested that the
606 runoff energy consumption of different landform units depends on gully type to some extent as well
607 as soil texture, slope and headwall height (Wells et al., 2009a). Besides, under this flow discharge
608 conditions, the proportion of energy consumption to the total flow energy ranged from 91.12% to
609 99.90%, indicating that almost all of flow energy was consumed during headcut erosion.
610 Furthermore, the proportion of energy consumption in UA, GH and GB was 15.6% - 19.8%, 77.3% -
611 78.6% and 2.8% - 5.8%, respectively (Fig. 9), which was also indirectly supported by the study of Su
612 et al. (2015) who suggested that the runoff energy consumption per unit soil loss from upstream area,
613 headcut and gully bed is 17.4%, 70.5% and 12.0%, respectively. This further signified that the gully
614 head consumed the most of runoff energy (77.5% on average) during headcut migration. The flow

615 energy must be consumed to surmount the soil resistance as headcut migrates, and the consumed
616 energy was mainly focused on headwall and plunge pool development (Alonso et al., 2002).

617 In terms of soil loss, our study indicated that the soil loss rate of the “UA-GH-GB” system
618 initially increased to the peak value and then gradually declined and stabilized (Fig. 10), which was
619 consistent with the results of many studies on rill and gully headcut erosion under different
620 conditions (slope, initial step height, flow discharge, soil type, soil stratification) (Bennett, 1999;
621 Bennett and Casalí, 2001; Gordon et al., 2007; Wells et al., 2009a; Shi et al., 2020a). Both the scour
622 depth and sediment production increased in the initial period of underlying surface adjustment, while
623 once the plunge pool development was maintained, and sediment yield decreased and gradually
624 stabilized (Bennett et al., 2000). In addition, the significant difference in soil loss process was found
625 among the three landform units. The soil loss of UA and GH decreased logarithmically over time,
626 which was similar with several studies (e.g., Su et al., 2015; Shi et al., 2020b). Nevertheless, the GB
627 was always characterized by sediment deposition for the inflow discharge of $< 4.8 \text{ m}^3 \text{ h}^{-1}$, whereas
628 the sediment was deposited firstly and then gradually transported as the inflow discharge increased to
629 6.0 and $7.2 \text{ m}^3 \text{ h}^{-1}$. Similar phenomena ~~was~~were also found in some previous studies on rill heacut
630 erosion (Bennett, 1999; Bennett and Casalí, 2001; Gordon et al., 2007; Wells et al., 2009a). This
631 further indicated that soil loss/deposition process of gully system was significantly influenced by
632 three landform units, and especially, the most of flow energy (77.5%) consumed at gully heads due to
633 jet flow erosion strongly weakened sediment transport capacity of flow on gully bed and thus
634 changed the soil loss/deposition process of gully system. However, Su et al. (2014, 2015) revealed a
635 larger soil loss volume or soil loss rate in gully bed than upstream area and headwall during bank
636 gully headcut erosion. This difference between our study and Su et al. (2014, 2015) is primarily
637 caused by the difference in slope gradient. The gully bed slope (20°) of bank gully was larger than
638 that (3°) of our study, indicating the runoff on gully bed of bank gully had stronger sediment
639 transport capacity (Zhang et al., 2009; Ali et a., 2013; Wu et al., 2016, 2018). Besides, some previous
640 also proved that the soil type, surface roughness, slope-length, groundwater/surface runoff were the
641 main factors influencing soil loss by gully erosion (Amare et al., 2020; Li et al., 2021). In view of the
642 proportion of soil loss, the proportion of UA and GH was 9.5% - 11.4% and 88.6% - 90.5%,

643 respectively, of which the proportion of deposited sediment on GB to the sediment yield from UA
644 and GH can reach up to 0.4% - 10.3%. This result fully demonstrated that the gully head is the main
645 source of sediment production during gully headcut erosion (Oostwoud-Wijdenes & Bryan, 1994;
646 Zhao, 1994; Su et al., 2014), and also manifested the necessary and importance of gully headcut
647 erosion controlling in gully-dominated region (Amare et al., 2019).

648 **4.3 Hydrodynamic characteristics of headcut erosion**

649 The significantly different relationships between soil loss and jet or hydraulic characteristics
650 were found among UA, GH, and GB. The soil loss rate of UA exponentially increased with five
651 hydraulic parameters (runoff velocity, Reynold number, Froude number, runoff shear stress and
652 stream power), indicating that soil loss of UA showed a stronger sensitive response to increasing
653 hydraulic properties. This could attribute to the frequent bank collapse on UA accelerating soil loss
654 (Wells et al., 2013; Qin et al., 2018). However, the sediment deposition rate of GB linearly decreased
655 with the five hydraulic parameters, signifying that sediment deposition on GB decreased at a stable
656 state with the increase of hydraulic parameters. Therefore, the sediment deposition rate would reach
657 zero when the five hydraulic parameters increased to the critical values, implying that the
658 transformation of sediment deposition to sediment transport on GB would be triggered. Furthermore,
659 the shear stress is the optimal parameter describing soil loss process of UA and GB, which differed
660 from some studies on hillslope/gully erosion hydrodynamic characteristics (Zhang et al., 2009; Shen
661 et al., 2019; Ma et al., 2020; Sidorchuk, 2020). Most of studies have verified that stream power is the
662 superior hydrodynamic parameter describing soil detachment process. This comparison also fully
663 illustrated the great difference in hydrodynamic characteristic between hillslope erosion and headcut
664 erosion. In this study, the soil loss of gully head (including plunge pool erosion) was significantly
665 affected by jet properties. It's confirmed that the plunge pool erosion by jet flow becomes a crucial
666 process controlling gully head migration and sediment production (Oostwoud-Wijdenes et al., 2000).
667 Consequently, the plunge pool erosion theory is usually employed to build several headcut retreat
668 models (Alonso et al., 2002; Campo-Bescós et al., 2013). Although the weak correlation between soil
669 loss of gully head and flow velocity at headcut breakpoint, the larger flow velocity resulted from
670 increasing inflow discharge would improve the shear stress of jet flow impinging gully bed, and thus

671 the gully headcut suffered stronger incisional erosion of the plunge pool. However, in fact, the soil
672 loss of gully head was also affected by on-wall flow erosion (Chen et al., 2013; Guo et al., 2021a),
673 and thus more studies should be conducted to clear the effect of on-wall flow properties on headwall
674 erosion.

675 From the energy consumption perspective, the soil loss rate of the three landform units
676 significantly and logarithmically increased with the energy consumption, and the similar change
677 trend was also found in the study of Su et al. (2015). This finding suggests that energy consumption
678 could be considered as the available parameter to estimate the soil loss of gully headcut erosion (Shi
679 et al., 2020b). Furthermore, we found the critical energy consumption initiating soil erosion of UA,
680 GH, and GB are 1.62 J s^{-1} , 5.79 J s^{-1} and 1.64 J s^{-1} , respectively, indicating the soil loss of gully head
681 (including plunge pool) needs more flow energy consumption (Zhang et al., 2018; Shi et al., 2020a,
682 2020b). This phenomenon can be attributed to the fact that the more runoff energy was consumed at
683 the gully headwall and plunge pool erosion than UA and GB and thus resulted in more severe soil
684 loss during headcut erosion. In addition, we found that the critical energy consumption activating soil
685 loss of “UA-GH-GB” system was lower the sum of critical energy consumption initiating soil loss
686 and sediment transport of three landform units (9.05 J s^{-1}). This result was closely related to mass
687 failures such as gully head and gully bank collapse can contribute the additional energy into the flow.
688 So, the role of gravitational erosion in controlling gully erosion process should be clarified in the
689 future studies.

690 **5 Implication, significance and limitations of this study**

691 Gully erosion has been studied for nearly a century, but its process and dynamic mechanism are
692 still difficult to clearly understand and reveal. Given this, our study attempted to clarify the
693 spatial-temporal changes in flow hydraulic characteristics, energy consumption and soil loss and
694 expound the response of soil loss to runoff properties and energy consumption during headcut
695 erosion through a series of simulation experiment under controlled conditions. These results could be
696 extended to wider conditions, such as gully scale, flow discharge determined by rainfall and drainage
697 area, which can promote the understanding of process and mechanism of gully erosion under real
698 ground conditions as well as the modelling and prediction of gully erosion. Especially, the variation

699 and proportion of energy consumption along “UA-GH-GB” in the process of gully erosion and its
700 influence on sediment yield were clearly elucidated in this study, which has an important guiding
701 significance for gully erosion control practice and restoration efforts. We can design some
702 engineering and/or vegetation measures at gully heads to pre-consume the most flow energy and the
703 energy dissipation structures could be designed and installed at the position where plunge pool
704 develops. Also, the appropriate size of these measures also can be determined to ensure the flow
705 energy of different landform units was lower than the corresponding critical energy consumption.

706 However, there are some potential limitations in our study. First, considering the complex
707 effects of lots of factors on gully erosion, the flow discharge upstream gully heads was designed as
708 the core factor affecting gully erosion in our study, and the five levels of flow discharge was
709 generated according to the rainfall, landform and gully morphology. But it is not really same as the
710 actual ground situations, such as the flow discharge upstream gully heads would not be constant
711 during a rainfall event. Second, it has not been confirmed how well our experimental results are in
712 line with the actual ground results. Therefore, further studies need to verify the experimental results
713 with the actual situations, so that the study results can be practiced and applied under actual rainfall
714 conditions. Third, in the future research, gully erosion experiments under different control measures
715 should be carried out to identify suitable gully erosion prevention measures. Although the
716 earlier-noted imperfection represents the limitation of our study, we still clearly demonstrated the
717 temporal-spatial change in hydraulic properties and soil loss during headcut erosion and quantify the
718 response relationships of soil loss of different landform units to energy consumption, which is of
719 great significance for deepening the understanding of the gully process and hydrodynamic
720 mechanism. Also, our results can provide valuable ideas and scientific basis for the construction of
721 gully erosion model and the design of gully erosion prevention measures.

722 **Summary**

723 This study investigated the temporal-spatial changes in flow hydraulic, energy consumption and
724 soil loss during headcut erosion based on a series of scouring experiments of gully headcut erosion.
725 The temporal changes in jet properties of gully head (GH) were significantly affected by upstream
726 inflow discharge. The upstream area (UA) and gully bed (GB) had similar temporal changes in

727 Reynold number, Froude number, shear stress and stream power. The flow was supercritical on UA,
728 but subcritical on GB, and the turbulent degree was enhanced by the increasing inflow discharge.
729 The presence of gully headwall significantly weakened flow Reynold number, shear stress and
730 stream power ~~decreased by 56.0%, 63.8% and 55.9%, respectively,~~ but lightly enhanced the Froude
731 number ~~increased by 7.9% when flow passed the gully headcut and plunge pool.~~ The accumulated
732 energy consumption at UA, GH and GB linearly increased with time. Overall, more than 91%91.12%
733 ~~99.90%~~ of total flow energy was consumed during headcut erosion, of which the GH accounted for
734 77.5% of the total runoff energy dissipation ~~followed by UA (18.3%) and GB (4.0%).~~ The soil loss of
735 UA and GH decreased logarithmically over time, whereas the GB was mainly characterized by
736 sediment deposition over time. The GH and UA contributed 88.5% and 11.5% of total soil loss,
737 respectively, of which 3.8% ~~sediment production~~soil loss was deposited on GB. The soil loss process
738 of UA and GH and the sediment deposition process of GB were significantly affected by flow
739 hydraulic and jet properties. Our study results revealed that the critical runoff energy consumption to
740 initiate soil erosion of UA, GH and GB are 1.62 J s^{-1} , 5.79 J s^{-1} and 1.64 J s^{-1} , respectively. The
741 runoff energy consumption ~~could~~should be considered as a non-negligible parameter to predict gully
742 headcut erosion.

743 **Data availability**

744 ~~At present, the original data are not publicly accessible because of a situation that we don't have~~
745 ~~permission to share data according to the requirement of the funded program and our institute.~~
746 ~~However, we are pleasure to share all data plotted in figures in this study for other colleagues.~~The
747 data that support the findings of this study are available from the first author
748 (guomingming@iga.ac.cn) and corresponding author upon request (nwafu_wwl@163.com).

749 **Author contribution**

750 Mingming Guo and Wenlong Wang designed the experiments. Mingming Guo, Zhuoxin Chen,
751 Tianchao Wang, Qianhua Shi, Man Zhao and Lanqian Feng carried out the experiments. Zhuoxin
752 Chen produced and processed the digital elevation model of erosion landform. Mingming Guo and

753 Wennlong Wang written and prepared the manuscript with contributions from all co-authors.

754 **Competing interests:**

755 The authors declare that they have no conflict of interest.

756 **Acknowledgments**

757 This work was supported by the National Natural Science Foundation of China (42077079,
758 41571275), the China Postdoctoral Science Foundation (2020M681062, [2021T140663](#)), and the
759 National Key Research and Development Program of China (2016YFC0501604). ~~Acknowledgement
760 for the data support from "Loess Plateau Data Center, National Earth System Science Data Sharing
761 Infrastructure, National Science & Technology Infrastructure of China. (<http://loess.geodata.cn>)"~~

762 **References**

- 763 Addisie, M.B., Ayele, G.K., Gessess, A.A., Tilahun, S.A., Zegeye, A.D., Moges, M.M., ... Steenhuis, T.S.:
764 Gully head retreat in the sub-humid Ethiopian Highlands: The Ene-Chilala catchment, *Land Degradation &*
765 *Development*, 28, 1579–1588, <https://doi.org/10.1002/ldr.2688>, 2017.
- 766 Ali, M., Seeger, M., Sterk, G., Moore, D.: A unit stream power based sediment transport function for overland
767 flow. *Catena*. 101, 197-204. <https://doi.org/10.1016/j.catena.2012.09.006>
- 768 Alonso, C.V., Bennett, S.J., Stein, O.R., 2002. Predicting head cut erosion and migration in concentrated flows
769 typical of upland areas, *Water Resources Research*, 38, 39-1–39-15, <http://dx.doi.org/10.1029/2001WR001173>,
770 2013.
- 771 Amare, S., Keesstra, S., van der Ploeg, M., Langendoen, E., Steenhuis, T., Tilahun, S.: Causes and controlling
772 factors of Valley bottom Gullies. *Land*, 8(9), 141, <https://doi.org/10.3390/land8090141>, 2019.
- 773 Amare, S., Langendoen, E., Keesstra, S., Ploeg, M. V. D., Gelagay, H., Lemma, H., van der Zee, S. E.:
774 Susceptibility to Gully Erosion: Applying Random Forest (RF) and Frequency Ratio (FR) Approaches to a
775 Small Catchment in Ethiopia. *Water*, 13(2), 216, <https://doi.org/10.3390/w13020216>, 2021.
- 776 Arabameri, A., Chen, W., Lombardo, L., Blaschke, T., Tien Bui, D.: Hybrid computational intelligence models
777 for improvement gully erosion assessment, *Remote Sensing*, 12(12), <https://doi.org/10.3390/rs12010140>, 140,
778 2020.
- 779 Battany, M.C., Grismer, M.E.: Rainfall runoff and erosion in Napa Valley vineyards: effects of slope, cover
780 and surface roughness, *Hydrological Processes*, 14(7), 1289-1304,
781 [https://doi.org/10.1002/\(SICI\)1099-1085\(200005\)14:7<1289::AID-HYP43>3.0.CO;2-R](https://doi.org/10.1002/(SICI)1099-1085(200005)14:7<1289::AID-HYP43>3.0.CO;2-R), 2015.
- 782 Beer, C.E., Johnson, H.P.: Factors in gully growth in the deep loess area of western Iowa. *Transactions of*
783 *ASAE*, 6, 237–240, <https://doi.org/10.13031/2013.40877>, 1963.
- 784 Belayneh, M., Yirgu, T., Tsegaye, D.: Current extent, temporal trends, and rates of gully erosion in the Gumara
785 watershed, northwestern Ethiopia, *Global Ecology and Conservation*, 24, e01255,
786 <https://doi.org/10.1016/j.gecco.2020.e01255>, 2020.

787 Bennett, S.J., Casali, J.: Effect of initial step height on headcut development in upland concentrated flows.
788 *Water Resources Research*, 37, 1475–1484, <https://doi.org/10.1029/2000WR900373>, 2001.

789 Bennett, S.J.: Effect of slope on the growth and migration of headcuts in rills, *Geomorphology*, 30, 273–290,
790 [https://doi.org/10.1016/S0169-555X\(99\)00035-5](https://doi.org/10.1016/S0169-555X(99)00035-5), 1999.

791 Bennett, S.J., Alonso, C.V.: Turbulent flow and bed pressure within headcut scour holes due to plane
792 reattached jets, *Journal of Hydraulic Research*, 44, 510–521, <https://doi.org/10.1080/00221686.2006.9521702>,
793 2006.

794 Bennett, S.J., Alonso, C.V., Prasad, S.N., Romkens, M.J.: Experiments on headcut growth and migration in
795 concentrated flows typical of upland areas, *Water Resources Research*, 36, 1911–1922,
796 <https://doi.org/10.1029/2000WR900067>, 2000.

797 Bogale, A. G., Aynalem, D. W., Adem, A. A., Mekuria, W., Tilahun, S.: Spatial and temporal variability of soil
798 loss in gully erosion in upper Blue Nile basin, Ethiopia, *Applied Water Science*, 10(5), 106,
799 <https://doi.org/10.1007/s13201-020-01193-4>, 2020.

800 Campo-Bescós, M.A., Flores-Cervantes, J.H., Bras, R.L., Casali, J., Giráldez, J.V.: Evaluation of a gully
801 headcut retreat model using multitemporal aerial photographs and digital elevation models, *Journal of*
802 *Geophysical Research: Earth Surface*, 118, 2159–2173, <https://doi.org/10.1002/jgrf.20147>, 2013.

803 Chaplot, V., Giboire, G., Marchand, P., Valentin, C.: Dynamic modelling for linear erosion initiation and
804 development under climate and land-use changes in northern Laos, *Catena*, 63, 318–328,
805 <https://doi.org/10.1016/j.catena.2005.06.008>, 2005.

806 Che, X.L.: Study of distribution characteristic and evolution of headward erosion on Dongzhi tableland of the
807 loess gully region, Yangling: Northwest A&F University, pp. 66-67, (In Chinese), 2012.

808 Chen, A., Zhang, D., Peng, H., Fan, J., Xiong, D., Liu, G.: Experimental study on the development of collapse
809 of overhanging layers of gully in Yuanmou Valley, China, *Catena*, 109, 177-185,
810 <https://doi.org/10.1016/j.catena.2013.04.002>, 2013.

811 De Baets, S., Poesen, J., Knapen, A., Galindo, P.: Impact of root architecture on the erosion-reducing potential
812 of roots during concentrated flow, *Earth Surface Processes and Landforms*, 32, 1323–1345,
813 <https://doi.org/10.1002/esp.1470>, 2007.

814 de Vente, J., Poesen, J.: Predicting soil erosion and sediment yield at the basin scale: Scale issues and
815 semi-quantitative models, *Earth-Science Reviews*, 71, 95–125, <https://doi.org/10.1016/j.earscirev.2005.02.002>,
816 2005.

817 DeLong, S.B., Johnson, J., Whipple, K.: Arroyo channel head evolution in a flash-flood-dominated
818 discontinuous ephemeral stream system, *Geological Society of America Bulletin*, 126, 1683–1701,
819 <https://doi.org/10.1130/B31064.1>, 2014.

820 Descroix, L., González Barrios, J.L., Viramontes, D., Poulénard, J., Anaya, E., Esteves, M., Estrada, J.: Gully
821 and sheet erosion on subtropical mountain slopes: their respective roles and the scale effect, *Catena*, 72, 325–
822 339, <https://doi.org/10.1016/j.catena.2007.07.003>, 2008.

823 Dotterweich, M., Rodzik, J., Zglobicki, W., Schmitt, A., Schmidtchen, G., Bork, H.R.: High resolution gully
824 erosion and sedimentation processes, and land use changes since the Bronze Age and future trajectories in the
825 Kazimierz Dolny area (Nałęczów Plateau, SE-Poland), *Catena*, 95, 50–62,
826 <https://doi.org/10.1016/j.catena.2012.03.001>, 2012.

827 Flores-Cervantes, J., Istanbuluoglu, E., Bras, R.: Development of gullies on the landscape: A model of
828 headcut retreat resulting from plunge pool erosion, *Journal of Geophysical Research*, 111, 1–14,
829 <https://doi.org/10.1029/2004JF000226>, 2006.

830 Frankl, A., Stal, C., Abraha, A., Nyssen, J., Rieke-Zapp, D., DeWulf, A., Poesen, J.: Detailed recording of
831 gully morphology in 3D through image-based modelling, *Catena*, 127, 92–101,
832 <https://doi.org/10.1016/j.catena.2014.12.016>, 2015.

833 Fu, B.J., Liu, Y., Lv, Y.H., He, C.S., Zeng, Y., Wu, B.F.: Assessing the soil erosion control service of
834 ecosystems change in the Loess Plateau of China, *Ecological Complexity*, 8, 284–293,
835 <https://doi.org/10.1016/j.ecocom.2011.07.003>, 2011.

836 Gordon, L.M., Bennett, S.J., Wells, R.R., Alonso, C.V.: Effect of soil stratification on the development and
837 migration of headcuts in upland concentrated flows, *Water Resources Research*, 43, W07412,
838 <https://doi.org/10.1029/2006WR005659>, 2007.

839 Guo, M., Wang, W., Shi, Q., Chen, T., Kang, H., Li, J.: An experimental study on the effects of grass root
840 density on gully headcut erosion in the gully region of China's Loess Plateau, *Land Degradation &
841 Development*, 30, 2107–2125, <https://doi.org/10.1002/ldr.3404>, 2019.

842 Guo, M., Wang, W., Wang, T., Wang, W., Kang, H.: Impacts of different vegetation restoration options on
843 gully head soil resistance and soil erosion in loess tablelands, *Earth Surface Processes and Landforms*, 45(4),
844 1038–1050, <https://doi.org/10.1002/esp.4798>, 2020a.

845 Guo, M.M., Wang, W.L., Kang, H.L., Yang, B.: Changes in soil properties and erodibility of gully heads
846 induced by vegetation restoration on the Loess Plateau, China, *Journal of Arid Land*, 10(5), 712–725,
847 <https://doi.org/10.1007/s40333-018-0121-z>, 2018.

848 Guo, M.M., Wang, W.L., Li, J.M., Bai, Y., Kang, H.L., Yang, B.: Runoff characteristics and soil erosion
849 dynamic processes on four typical engineered landforms of coalfields: An in-situ simulated rainfall
850 experimental study, *Geomorphology*, 349, 106896, <https://doi.org/10.1016/j.geomorph.2019.106896>, 2020b.

851 Guo, M.M., Lou, Y.B., Chen, Z.X., Wang, W.L., Feng, L.Q., Zhang, X.Y.: The proportion of jet flow and
852 on-wall flow and its effects on soil loss and plunge pool morphology during gully headcut erosion, *Journal of
853 Hydrology*, 598, 126220, <https://doi.org/10.1016/j.jhydrol.2021.126220>, 2021a.

854 Guo, M.M., Chen, Z.X., Wang, W.L., Wang, T.C., Wang, W.X., Cui, Z.Q.: Revegetation induced change in
855 soil erodibility as influenced by slope situation on the Loess Plateau, *Science of the Total Environment*, 772,
856 145540, <https://doi.org/10.1016/j.scitotenv.2021.145540>, 2021b.

857 Hager, W.H.: Hydraulics of plane free overfall, *Journal of Hydraulic Engineering*, 109, 1683–1697,
858 [https://doi.org/10.1061/\(ASCE\)0733-9429\(1983\)109:12\(1683\)](https://doi.org/10.1061/(ASCE)0733-9429(1983)109:12(1683)), 1983.

859 Hanson, G.J., Robinson, K.M., Cook, K.R.: Prediction of headcut migration using a deterministic approach,
860 *Transactions of the ASAE*, 44(4), 525–531, <https://doi.org/10.13031/2013.6112>, 2001.

861 Hosseinalizadeh, M., Kariminejad, N., Chen, W., Pourghasemi, H.R., Alinejad, M., Behbahani, A.M.,
862 Tiefenbacher, J.P.: Gully headcut susceptibility modeling using functional trees, naïve Bayes tree, and random
863 forest models, *Geoderma*, 342, 1–11, <https://doi.org/10.1016/j.geoderma.2019.01.050>, 2019.

864 Ionita, I.: Gully development in the Moldavian Plateau of Romania, *Catena*, 68, 133–140,
865 <https://doi.org/10.1016/j.catena.2006.04.008>, 2006.

866 Ionita, I., Niacsu, L., Petrovici, G., Blebea-Apostu, A.M.: Gully development in eastern Romania: a case study
867 from Falciu Hills, *Natural Hazards*, 79, 113–138, <https://doi.org/10.1007/s11069-015-1732-8>, 2015.

868 Jiang, Y., Shi, H., Wen, Z., Guo, M., Zhao, J., Cao, X., Fan, Y., Zheng, C.: The dynamic process of slope rill
869 erosion analyzed with a digital close range photogrammetry observation system under laboratory conditions,
870 *Geomorphology*, 350,106893, <https://doi.org/10.1016/j.geomorph.2019.106893>, 2020.

871 Jiao, J.Y., Wang, W.Z., Hao, X.P.: Precipitation and erosion characteristics of rainstorm in different pattern on
872 Loess Plateau, *Journal of Arid Land Resources and Environment*, 13(1), 34-42, (In Chinese), 1999.

873 Kirkby, M.J., Bull, L.J., Poesen, J., Nachtergaele, J., Vandekerckhove, L.: Observed and modelled
874 distributions of channel and gully heads—with examples from SE Spain and Belgium, *Catena*, 50, 415–434,
875 [https://doi.org/10.1016/S0341-8162\(02\)00128-5](https://doi.org/10.1016/S0341-8162(02)00128-5), 2003.

876 Li, Binbing., Huang, Lei., Feng, Lin., Li, Peng., Yao, Jingwei., Liu, Fangming., Li, Junli., Tang, Hui.: Gully
877 sidewall expansion process on loess hill slope erosion, *Journal of Basic Science and Engineering*, 24(6),
878 1147-1158. (In Chinese), 2016.

879 Li, H., Cruse, R.M., Liu, X.B., Zhang, X.Y.: Effects of topography and land use change on gully development
880 in typical Mollisol region of Northeast China, *Chinese Geographical Science*, 26, 779-788,
881 <https://doi.org/10.1007/s11769-016-0837-7>, 2016.

882 Li, M., Song, X.Y., Shen, B., Li, H.Y., Meng, C.X.: Influence of vegetation change on producing runoff and
883 sediment in gully region of Loess Plateau, *Journal of Northwest Sci-Tech University of AgricuUAure and*
884 *Forestry (Natural Science Edition)*, 34, 117-120, (In Chinese), 2006.

885 Li, Y., Mo, Y. Q., Are, K. S., Huang, Z., Guo, H., Tang, C., Abegunrin, T.P., Qin, Z.H, Kang, Z.W., Wang, X.:
886 Sugarcane planting patterns control ephemeral gully erosion and associated nutrient losses: Evidence from
887 hillslope observation. *Agriculture, Ecosystems & Environment*, 309, 107289,
888 <https://doi.org/10.1016/j.agee.2020.107289>, 2021.

889 Li, Z., Zhang, Y., Zhu, Q., He, Y., Yao, W.: Assessment of bank gully development and vegetation coverage on
890 the Chinese Loess Plateau, *Geomorphology*, 228, 462–469, <https://doi.org/10.1016/j.geomorph.2014.10.005>,
891 2015.

892 Li, Z., Zheng, F.L., Liu, W.Z., Flanagan, D.C.: Spatial distribution and temporal trends of extreme temperature
893 and precipitation events on the Loess Plateau of China during 1961–2007, *Quaternary International*, 226(1-2),
894 92-100, <https://doi.org/10.1016/j.quaint.2010.03.003>, 2010.

895 Ma, Q., Zhang, K., Cao, Z., Wei, M., & Yang, Z.: Soil detachment by overland flow on steep cropland in the
896 subtropical region of China, *Hydrological Processes*, 34(8), 1810-1820, <https://doi.org/10.1002/hyp.13694>,
897 2020

898 Martínez-Casasnovas, J.A., Concepción Ramos, M., García-Hernández, David.: Effects of land - use
899 changes in vegetation cover and sidewall erosion in a gully head of the Penedès region (northeast Spain),
900 *Earth Surface Processes & Landforms*, 34, 1927-1937, <https://doi.org/10.1002/esp.1870>, 2009.

901 Nazari Samani, A., Ahmadi, H., Mohammadi, A., Ghoddousi, J., Salajegheh, A., Boggs, G., Pishyar, R.:
902 Factors Controlling Gully Advancement and Models Evaluation (Hableh Rood Basin, Iran), *Water Resources*
903 *Management*, 24, 1532–1549, <https://doi.org/10.1007/s11269-009-9512-4>, 2010.

904 Oostwoud-Wijdenes, D., Bryan, R.B.: The significance of gully headcuts as a source of sediment on low-angle
905 slopes at Baringo, Kenya, and initial control measures, *Advances in Geocology*, 27, 205–231, 1994.

906 Oostwoud-Wijdenes, D., Poesen, J., Vandekerckhove, L., Ghesquiere, M.: Spatial distribution of gully head
907 activity and sediment supply along an ephemeral channel in a Mediterranean environment, *Catena*, 39, 147–
908 167, [http://202.194.143.28:80/rwt/SD/https/MSYXTLUQPJUB/10.1016/S0341-8162\(99\)00092-2](http://202.194.143.28:80/rwt/SD/https/MSYXTLUQPJUB/10.1016/S0341-8162(99)00092-2), 2000.

909 Pan, C., Ma, L., Wainwright, J., Shangguan, Z.: Overland flow resistances on varying slope gradients and
910 partitioning on grassed slopes under simulated rainfall, *Water Resources Research*, 52, 2490–2512,
911 <https://doi.org/10.1002/2015WR018035>, 2016.

912 Poesen, J., Nachtergaele, J., Verstraeten, G., Valentin, C.: Gully erosion and environmental change:
913 Importance and research needs, *Catena*, 50, 91-133, [https://doi.org/10.1016/S0341-8162\(02\)00143-1](https://doi.org/10.1016/S0341-8162(02)00143-1), 2003.

914 Qin, Chao., Zheng, Fenli., Wells Robert, R., Xu, Ximeng, Wang, Bin., Zhong, Keyuan.: A laboratory study of
915 channel sidewall expansion in upland concentrated flows, *Soil and Tillage Research*, 178, 22-31,
916 <https://doi.org/10.1016/j.still.2017.12.008>, 2018.

917 Reuter, H.I., Nelson, A., Jarvis, A.: An evaluation of void filling interpolation methods for SRTM data,
918 *International Journal of Geographic Information Science*, 21(9), 983-1008, 2007.

919 Rieke-Zapp, D.H., Nichols, M.H.: Headcut retreat in a semiarid watershed in the southwestern United States
920 since 1935, *Catena*, 87, 1–10, <https://doi.org/10.1016/j.catena.2011.04.002>, 2011.

921 Rodzik, J., Furtak, T., Zglobicki, W.: The impact of snowmelt and heavy rainfall runoff on erosion rates in a
922 gully system, Lublin Upland, Poland, *Earth Surface Processes & Landforms*, 34, 1938–1950,
923 <https://doi.org/10.1002/esp.1882>, 2009.

924 Rouse, H.: *Engineering hydraulics*. Hoboken, NJ: Wiley, 1950.

925 Sanchis, M.P., Torri, D., Borselli, L., Poesen, J.: Climate effects on soil erodibility, *Earth Surface Processes &*
926 *Landforms*, 33, 1082–1097, <https://doi.org/10.1002/esp.1604>, 2008.

927 Shen, N., Wang, Z., Zhang, Q., Chen, H., Wu, B.: Modelling soil detachment capacity by rill flow with
928 hydraulic variables on a simulated steep loessial hillslope, *Hydrology Research*, 50(1), 85-98,
929 <https://doi.org/10.2166/nh.2018.037>, 2018.

930 Shi, Q.H., Wang, W.L., Guo, M.M., Chen, Z.X., Feng, L.Q., Zhao, M., Xiao, H.: The impact of flow discharge
931 on the hydraulic characteristics of headcut erosion processes in the gully region of the Loess Plateau,
932 *Hydrological processes*, 34, 718-729, <https://doi.org/10.1002/hyp.13620>, 2020.

933 Shi, Q., Wang, W., Zhu, B., Guo, M.: Experimental study of hydraulic characteristics on headcut erosion and
934 erosional response in the tableland and gully regions of China, *Soil Science Society of America Journal*, 84,
935 700–716, <https://doi.org/10.1002/saj2.20068>, 2020.

936 Sidorchuk, A.: The potential of gully erosion on the Yamal peninsula, West Siberia. *Sustainability*, 12(1), 260,
937 <https://doi.org/10.3390/su12010260>, 2020.

938 Stein, O., Julien, P., Alonso, C.: Mechanics of jet scour downstream of a headcut, *Journal of Hydraulic*
939 *Research*, 31, 723–738, <https://doi.org/10.1080/00221689309498814>, 1993.

940 Su, Z.A., Xiong, D.H., Dong, Y.F., Zhang, B.J., Zhang, S., Zheng, X.Y., Fang, H.D.: Hydraulic properties
941 of concentrated flow of a bank gully in the dry - hot valley region of southwest China, *Earth Surface*
942 *Processes and Landforms*, 40, 1351 - 1363. <https://doi.org/10.1002/esp.3724>, 2015.

943 Su, Z.A., Xiong, D.H., Dong, Y.F., Li, J.J., Yang, D., Zhang, J.H., He, G.X.: Simulated headward erosion of
944 bank gullies in the Dry-hot Valley Region of southwest China, *Geomorphology*, 204, 532–541,
945 <https://doi.org/10.1016/j.geomorph.2013.08.033>, 2014.

946 Sun, W.Y., Mu, X.M., Song, X.Y., Wu, D., Cheng, A.F., Qiu, B.: Changes in extreme temperature and
947 precipitation events in the Loess Plateau (China) during 1960–2013 under global warming, *Atmospheric*
948 *Research*, 168, 33-48, <https://doi.org/10.1016/j.atmosres.2015.09.001>, 2016.

949 Thompson, J.R.: Quantitative effect of watershed variables on rate of gully - head advancement. *Transactions*
950 *of the ASABE*, 7, 54 - 55, <https://doi.org/10.13031/2013.40694>, 1964.

951 Torri, D., Poesen, J.: A review of topographic threshold conditions for gully head development in different
952 environments, *Earth-Science Reviews*, 130, 73–85, <https://doi.org/10.1016/j.earscirev.2013.12.006>, 2014.

953 Valentin, C., Poesen, J., Li, Y.: Gully erosion: Impacts, factors and control, *Catena*, 63, 132–153,
954 <https://doi.org/10.1016/j.catena.2005.06.001>, 2005.

955 Vandekerckhove, L., Poesen, J., Govers, G.: Medium-term gully headcut retreat rates in southeast Spain
956 determined from aerial photographs and ground measurements, *Catena*, 50(2-4), 329-352,
957 [https://doi.org/10.1016/S0341-8162\(02\)00132-7](https://doi.org/10.1016/S0341-8162(02)00132-7), 2003.

958 Vandekerckhove, L., Poesen, J., Wijdenes, D.O., Nachtergaele, J., Tomás de Figueiredo.: Thresholds for gully
959 initiation and sedimentation in Mediterranean Europe, *Earth Surface Processes & Landforms*, 25(11),
960 1201-1220, [https://doi.org/10.1002/1096-9837\(200010\)25:11<1201::AID-ESP131>3.0.CO;2-L](https://doi.org/10.1002/1096-9837(200010)25:11<1201::AID-ESP131>3.0.CO;2-L), 2015.

961 Vanmaercke, M., Poesen, J., Mele, B.V., Demuzere, M., Bruynseels, A., Golosov, V., ... Yermolaev, O.: How
962 fast do gully headcuts retreat?, *Earth - Science Reviews*, 154, 336 - 355,
963 <https://doi.org/10.1016/j.earscirev.2016.01.009>, 2016.

964 Vannoppen, W., Vanmaercke, M., De Baets, S., Poesen, J.: A review of the mechanical effects of plant roots on
965 concentrated flow erosion rates, *Earth - Science Reviews*, 150, 666 - 678,
966 <https://doi.org/10.1016/j.earscirev.2015.08.011>, 2015.

967 Vanwalleghe, T., Bork, H.R., Poesen, J., Schmidtchen, G., Dotterweich, M., Nachtergaele, J., Bork, H.,
968 Deckers, J., Brüsch, B., Bungeneers, J., De Bie, M.: Rapid development and infilling of a buried gully under
969 cropland, Central Belgium, *Catena*, 63, 221–243, <https://doi.org/10.1016/j.catena.2005.06.005>, 2005.

970 Vanwalleghe, T., Van Den Eeckhaut, M., Poesen, J., Deckers, J., Nachtergaele, J., Van Oost, K., Slenters, C.:
971 Characteristics and controlling factors of old gullies under forest in a temperate humid climate: a case study
972 from the Meerdaal Forest (Central Belgium), *Geomorphology*, 56(1), 15–29,
973 [https://doi.org/10.1016/S0169-555X\(03\)00043-6](https://doi.org/10.1016/S0169-555X(03)00043-6), 2003.

974 Wells, R.R., Alonso, C.V., Bennett, S.J.: Morphodynamics of Headcut Development and Soil Erosion in
975 Upland Concentrated Flows, *Soil Science Society of America Journal*, 73, 521–530.
976 <https://doi.org/10.2136/sssaj2008.0007>, 2009a.

977 Wells, R.R., Bennett, S.J., Alonso, C.V.: Effect of soil texture, tailwater height, and pore - water pressure on
978 the morphodynamics of migrating headcuts in upland concentrated flows, *Earth Surface Processes and
979 Landforms*, 34, 1867 - 1877, <https://doi.org/10.1002/esp.1871>, 2009b.

980 Wells, R.R., Momm, H.G., Rigby, J.R., Bennett, S.J., Bingner, R.L., Dabney, S.M.: An empirical investigation
981 of gully widening rates in upland concentrated flows, *Catena*, 101, 114-121,
982 <https://doi.org/10.1016/j.catena.2012.10.004>, 2013.

983 Wen, X., Wu, X., Gao, M.: Spatiotemporal variability of temperature and precipitation in Gansu province
984 (northwest China) during 1951–2015, *Atmospheric Research*, 197, 132-149,
985 <https://doi.org/10.1016/j.atmosres.2017.07.001>, 2017.

986 Wen, Y., Kasielke, T., Li, H., Zhang, B., Zepp, H.: May agricultural terraces induce gully erosion? a case study
987 from the black soil region of northeast China. *Science of The Total Environment*, 750(4), 141715,
988 <https://doi.org/10.1016/j.scitotenv.2020.141715>, 2020.

989 Wu, Bing., Wang, Zhanli., Zhang, Qingwei., Shen, Nan., Liu, June., Wang, Sha.: Evaluation of shear stress
990 and unit stream power to determine the sediment transport capacity of loess materials on different slopes,
991 *Journal of Soil & Sediments*, 18, 116–127, <https://doi.org/10.1007/s11368-017-1758-5>, 2018.

992 Wu, B., Wang, Z., Shen, N., Wang, S.: Modelling sediment transport capacity of rill flow for loess sediments
993 on steep slopes, *Catena*, 147, 453-462, <https://doi.org/10.1016/j.catena.2016.07.030>, 2016.

994 Xia, L., Song, X.Y., Fu, N., Li, H.Y., Li, Y.L.: Impacts of land use change and climate variation on green water
995 in the Loess Plateau Gully Region—A case study of Nanxiaohegou basin, *Journal of Hydraulic Engineering*,
996 48(6), 678-688, (In Chinese), 2017.

997 Xu, J.Z., Li, H., Liu, X.B., Hu, W., Yang, Q.N., Hao, Y.F., Zhen, H.C., Zhang, X.Y.: Gully Erosion Induced by
998 SnowmeUA in Northeast China: A Case Study, *Sustainability*, 11, <https://doi.org/10.3390/su11072088>, 2019.

999 Xu, X.M., Zheng, F.L., Wilson, G.V., Wu, M.: Upslope inflow, hillslope gradient and rainfall intensity impacts
1000 on ephemeral gully erosion, *Land Degradation & Development*, 28, 2623-2635
1001 <https://doi.org/10.1002/ldr.2825>, 2017.

1002 Xu, X.M., Zheng, F.L., Qin, C., Wu, H.Y., Wilson, G.V.: Impact of cornstalk buffer strip on hillslope soil
1003 erosion and its hydrodynamic understanding, *Catena*, 149, 417-425,
1004 <https://doi.org/10.1016/j.catena.2016.10.016>, 2017.

1005 Xu, X.M., Wang, H.B., Zhao, J.Y., Liu, X.J.: Dynamic variation of soil erosion of Nanxiaohegou small
1006 watershed during 2004-2016, *Soil and Water Conservation in China*, 443(2), 59-61, (In Chinese), 2019.

1007 Yang, C.T.: Potential energy and stream morphology, *Water Resource Research*, 7(2), 311-223,
1008 <https://doi.org/10.1029/WR007i002p00311>, 1971a.

1009 Yang, C.T.: On river meanders, *Journal of Hydrology*, 13, 231-253,
1010 [https://doi.org/10.1016/0022-1694\(71\)90226-5](https://doi.org/10.1016/0022-1694(71)90226-5), 1971b.

1011 Zhang, B.J., Xiong, D.H., Su, Z.A., Yang, D., Dong, Y.F., Xiao, L., Zhang, S., Shi, L.T.: Effects of initial step
1012 height on the headcut erosion of bank gullies: a case study using a 3D photo-reconstruction method in the
1013 Dry-hot Valley region of southwest China, *Physical Geography*, 37, 409-429,
1014 <https://doi.org/10.1080/02723646.2016.1219939>, 2016.

1015 Zhang, B.J., Xiong, D.H., Zhang G.H., Zhang, S., Wu, H., Yang, D., Xiao, L., Dong, Y.F., Su, Z.A., Lu, X.N.:
1016 Impacts of headcut height on flow energy, sediment yield and surface landform during bank gully erosion
1017 processes in the Yuanmou Dry - hot Valley region, southwest China, *Earth Surface Processes & Landforms*,
1018 43(10), 2271-2282, <https://doi.org/10.1002/esp.4388>, 2018.

1019 Zhang, H.X.: The characteristics of hard rain and its distribution over the Loess Plateau, *Acta Geographica*
1020 *Sinica*, 38, 416-425, (In Chinese), 1983.

1021 Zhang, G.H., Liu, Y.M., Han, Y.F., Zhang, X.C.: Sediment transport and soil detachment on steep slopes: I.
1022 transport capacity estimation, *Soil Science Society of America Journal*, 73, 1291-1297,
1023 <https://doi.org/10.2136/sssaj2008.0145>, 2009.

1024 Zhang, X., Fan, J., Liu, Q., Xiong D.: The contribution of gully erosion to total sediment production in a small
1025 watershed in Southwest China, *Physical Geography*, 39(3), 1-18,
1026 <https://doi.org/10.1080/02723646.2017.1356114>, 2018.

1027 Zhao, A.C.: Analysis of control models of typical small watershed in gully area of Loess Plateau, the east part
1028 of Gansu Province, *Research of Soil and Water Conservation*, 1, 45-49, (In Chinese), 1994.

1029 Zhu, T.X.: Gully and tunnel erosion in the hilly Loess Plateau region, China, *Geomorphology*, 153, 144-155,
1030 <https://doi.org/10.1016/j.geomorph.2012.02.019>, 2012.